

9950-990

DRL No. 216
DRD No. SE-3

DOE/JPL 956831-2
Distribution Category UC-63

ARCO Solar, Inc.

Quarterly Report No. 2

**PULSED EXCIMER LASER PROCESSING
FOR COST-EFFECTIVE SOLAR CELLS**

JPL Contract No. 956831

Reporting Period: August - October 1984

(NASA-CR-175465) PULSED EXCIMER LASER
PROCESSING FOR COST-EFFECTIVE SOLAR CELLS
Quarterly Report, Aug. - Oct. 1984 (ARCO
Solar, Inc.) SE & HC A4/EF A01 CSCI 10A

NE5-19520

Unclas
G3/44 14309

Prepared for

**California Institute of Technology
Jet Propulsion Laboratory
4800 Oak Grove Drive
Pasadena, California 91109**

Submitted by

**ARCO Solar, Inc.
P. O. Box 2105
Chatsworth, California 91313**



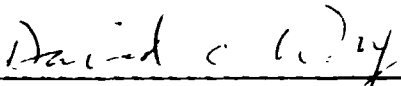
DRL No. 216
DRD No. SE-3

DOE/JPL 956831-2
Distribution Category UC-63

**PULSED EXCIMER LASER PROCESSING
FOR COST-EFFECTIVE SOLAR CELLS**

**Quarterly Report No. 2
August - October 1984**

Prepared By



D. Wong
Principal Investigator

Approved By



W. R. Bottenberg
Program Manager

ARCO Solar, Inc.
P. O. Box 2105
Chatsworth, California 91313

The JPL Flat-Plate Solar Array Project is sponsored by the U.S. Department of Energy and forms part of the solar Photovoltaic Conversion Program to initiate a major effort toward the development of low-cost solar arrays. This work was performed for the Jet Propulsion Laboratory, California Institute of Technology, by agreement between NASA and DOE.

This work was performed for the Jet Propulsion Laboratory, California Institute of Technology, and was sponsored by the U.S. Department of Energy through an agreement with the National Aeronautics and Space Administration.

This report was prepared as an account of work sponsored by an agency of the United States Government. Neither the United States Government nor any agency thereof, nor any of their employees, makes any warranty, express or implied, or assumes any legal liability or responsibility for the accuracy, completeness or usefulness of any information, apparatus, product or process disclosed, or represents that its use would not infringe privately owned rights.

Reference herein to any specific commercial product, process, or service by trade name, trademark manufacturer, or otherwise, does not necessarily constitute or imply its endorsement, recommendation, or favoring by the United States Government or any agency thereof. The views and opinions of authors expressed herein do not necessarily state or reflect those of the United States Government or any agency thereof.

ABSTRACT

Junction formation optimization has been the focus of activity. Improved cell efficiency was demonstrated by use of a large beam size laser of more homogeneous output. However, the cost of operating such a high power laser is presently considered too large for production use. Its slow processing speed (30 pulses per hour) had also retarded experimentation.

During this quarter, a smaller laser was reactivated with the installation of homogenizing lenses to produce more uniform and reproducible beam output. The highest Cz cell efficiency obtained was above 15.8%. Factors which presently limit efficiency include non-ideal ion implant potential for shallow junction formation, insufficient beam homogeneity, and metallization shadowing. Wafer surface condition before laser annealing has been found to affect cell performance.

CONTENTS

1.0	Introduction.....	1-1
2.0	Experimental Progress.....	2-1
2.1	Laser Equipment Status and Improvement.....	2-1
2.1.1	Beam Profiling of Large Laser.....	2-1
2.1.2	Beam Uniformity of Small Laser and Improvements.....	2-2
2.1.3	Laser Annealing of Ion Implanted Wafers.....	2-8
2.1.4	Optical Transport and Beam Shaping for Surface Passivation and Metallization Process Steps.....	2-14
2.2	Ion Implantation.....	2-14
2.2.1	Glow Discharge Ion Implantation.....	2-14
2.2.2	Ion Gun Implantation.....	2-16
2.2.3	Ion Milling Implantation.....	2-16
2.3	Laser-Assisted CVD Equipment.....	2-17
3.0	Experimental.....	3-1
3.1	Cell Processing by Large Laser, "Lucy".....	3-1
3.2	Cell Processing by Small Laser, "Exci-Lite 1".....	3-4
3.2.1	p-Type Substrate With 31p+ Ion Implant Dopant.....	3-4
3.2.2	n-Type Substrate With 11B+ Ion Implant Dopant.....	3-11
4.0	Discussion.....	4-1
4.1	Laser Annealing Processing.....	4-1
4.2	Substrates: p or n Type	4-5

PRECEDING PAGE BLANK NOT FILMED

CONTENTS (continued)

5.0	Process Selection Revision and Sensitivity Analysis.....	5-1
5.1	Revised Process.....	5-1
5.2	Process Sensitivity Assessment.....	5-1
6.0	Conclusion.....	6-1
7.0	Problems and Plans.....	7-1
7.1	Problems.....	7-1
7.2	Plans.....	7-1
	References.....	8-1
	Acknowledgments.....	9-1

Tables

2-1.	Large laser annealing parameters.....	2-10
2-2.	Small laser annealing parameters.....	2-11
3-1.	Electrical performance of "Lucy" processed Cz cells.....	3-2
3-2.	Laser annealing by large laser.....	3-3
3-3.	Laser annealing by improved small laser.....	3-5
3-4.	Sheet resistivity of wafers.....	3-9
3-5.	Electrical performance of B24 cells.....	3-10
3-6.	Small laser annealing of Cz and FZ wafers.....	3-12
3-7.	ASEC-coated Cz cells	3-14
3-8.	n-type substrates processed by large laser.....	3-15
3-9.	n-type substrates processed by small laser.....	3-16

CONTENTS (continued)

Figures

2-1.	Optical layout of small laser.....	2-2
2-2.	Beam profile after kaleidoscope homogenization.....	2-4
2-3.	Output beam with no external aperture.....	2-4
2-4.	Optical systems studied by ray tracing.....	2-6
2-5.	Spot diagram at front surface of kaleidoscope.....	2-7
2-6.	Spot diagram at kaleidoscope exit plane.....	2-7
2-7.	Case 1: Single 13 mm lens.....	2-7
2-8.	Case 2: Results obtained by using two biconvex lenses.....	2-9
2-9.	Case 3: Spot diagram at image plane.....	2-9
2-10.	Demonstration of edge fall-off of laser spot.....	2-10
2-11.	Excimer laser pulse waveforms.....	2-12
2-12.	Schematic of glow discharge implantation chamber.....	2-15
2-13.	Quartz envelope inside implantation chamber.....	2-16
2-14.	Gas cabinet schematic.....	2-17
3-1.	Surface contamination.....	3-6
3-2.	Laser scan showing incomplete surface annealing.....	3-7
3-3.	Surface damage revealed by etching.....	3-8
3-4.	I-V curves of best cell.....	3-13
3-5.	Spectral response of best cell.....	3-14
3-6.	Depth profiles.....	3-17
4-1.	Decrease in beam demarcation lines during the past four months.....	4-2

CONTENTS (continued)

4-2.	Laser scan showing edge damage.....	4-3
4-3.	Damage caused by various pulse shapes.....	4-4
5-1.	Revised excimer laser process.....	5-2
7-1.	Program schedule.....	7-2

SECTION 1.0 INTRODUCTION

After severe surface damage due to beam nonuniformity of the small laser was observed, a more powerful excimer laser was used at 308 nm to anneal 5 keV phosphorus ion implanted wafers with an increase of energy density in order to achieve greater depth of annealing. The onset of surface damage was seen at an energy density of above 2.0 J/cm^2 with pulse duration near 80 nsec. The best cell efficiencies fell short of the goal, with 9.5% observed before antireflection (AR) coat, whereas 11.5% is required. Two major reasons for this shortfall were identified. One reason is the use of phosphorus ion implant energies of 5 keV or more, which causes the phosphorus to penetrate more than 0.2 microns. Laser annealing further increases the dopant depth, making it difficult to obtain a shallow junction. The second and more important reason is nonuniformity in the laser beam spatial intensity profiles that require high overlap factors to compensate beam inhomogeneity.

Being larger in beam cross section and with more uniform output than the smaller laser, the large laser demonstrated comparatively higher efficiency cells. However, homogenizing the smaller laser beam by kaleidoscope decreased surface damage and thus helped to improve V_{oc} and fill factor. Cell efficiency as high as 15.8% was obtained with Cz wafers processed by the improved small laser at energy density of about 1.4 J/cm^2 with 50% overlap.

To achieve the goal of 16.5%, it is felt necessary to have a dependable ion implant of low energy and high dosage. An implanter utilizing the glow discharge concept is being fabricated. The unit would provide 1-5 keV with dosage as high as $1 \times 10^{16} \text{ atoms/cm}^2$.

Equipment for laser-assisted fine gridline CVD deposition has been designed and fabrication is progressing. In the meantime, fine gridlines that allow 96% active area will be processed by photolithographic techniques.

SECTION 2.0 EXPERIMENTAL PROGRESS

2.1 LASER EQUIPMENT STATUS AND IMPROVEMENT

In order to obtain better laser beam uniformity for use in the junction formation process step, an optical beam homogenizer was introduced in the beam line of the small excimer laser. Good spatial uniformity was achieved. In addition, the pulse modulator configuration of the small laser was modified to increase laser output energy to 25 mJ and to extend the laser pulse duration to 30 nsec.

A number of p-type wafers were processed at various values of laser energy density and spatial overlap. It was found that good solar cells (0.611 V and 9.7% efficiency before AR coating) could be obtained with 50% overlap and an energy density of 1.4 J/cm² for the 30 nsec pulse duration used. At higher energy, the wafer surface is damaged, whereas at lower energy the annealing is incomplete.

Difficulty was encountered in establishing reproducible results. The damage threshold and junction annealing threshold energy density have been found to vary with the specific time history of the laser pulse and with the sharpness of focus of the square spot on the wafer. In addition the shot-to-shot reproducibility of the laser deteriorated and was corrected.

2.1.1 Beam Profiling of Large Laser

An effort was initiated to measure the large laser ("Lucy") intensity profile using the reticon array. Unfortunately, due to the presence of the high voltage switches and the e-beam discharge, electrical noise prevented successful operation of the unshielded array and computer. Due to the high speed signals present on the reticon array board, cable lengths are limited and thus both array and motherboard must be located less than 3' from the actual location chosen for beam profiling. It is not practical to relay the image of the output aperture to the existing screen room.

A portable Faraday enclosure is being built for both the reticon array and computer so that the profiling of the large beam can be completed. The enclosure will contain the array board mounted on a two-axis translational stage. All signal and power cables will be grounded at the main screen room. Multiple (1024 points) shots at a single 3x3 mm location will be obtained to determine pulse-to-pulse variation. A complete (~12000 points) profile of the beam will also be obtained to determine edge sharpness and overall uniformity.

Two 5x5x100 mm kaleidoscopes are available for use to improve the

uniformity of the beam from the large laser. However, actual testing has not been performed yet as most of the later experiments have concentrated on the small laser.

2.1.2 Beam Uniformity of Small Laser and Improvements

To improve the spatial uniformity of the beam of the small excimer laser (Exci-Lite 1), three small ($\sim 1.7 \times 1.7 \times 100$ mm) kaleidoscopes were purchased. One was mounted in a five-axis (three translation plus two angles) holder; the other two kaleidoscopes were set aside as spares. The holder was designed to support the kaleidoscope on thin wires near each end of the kaleidoscope. This resulted in the correct index of refraction conditions for total internal reflection along the entire length of the kaleidoscope and hence optimal light throughput. A section of rectangular channel tubing surrounds the kaleidoscope and serves to protect three of its long optical surfaces. Propagation of the beam through the kaleidoscope can be observed through the one exposed surface and the exposed ends. The optical arrangement is shown in Fig. 2-1. Alignment is performed using the same HeNe laser beam that is used to align the excimer laser cavity, thus ensuring colinearity. The light throughput using this set-up was found to be 78% with the input beam focused very close to the front surface of the light pipe. This throughput is measured for a single input lens and kaleidoscope, or a total of four optical surfaces. The theoretical value based on Fresnel losses is 81.5% so it is very close to the maximum

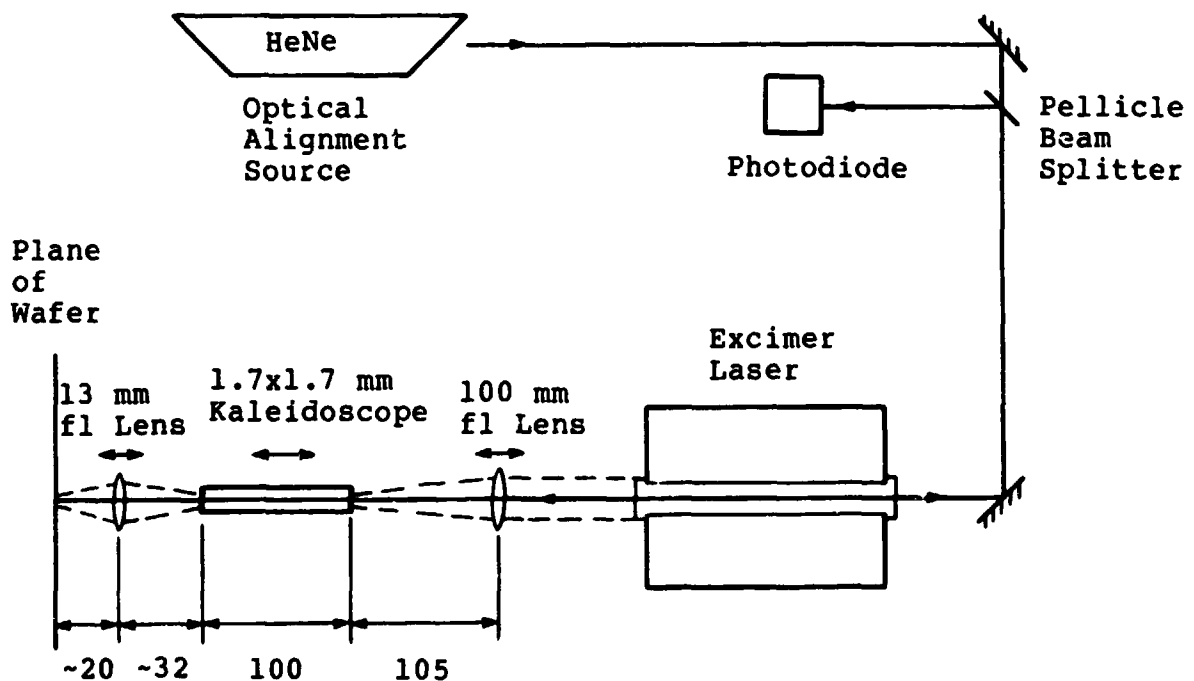


Fig. 2-1. Optical layout of small laser.

expected value. For reasons to be discussed, such optimal focusing could not be implemented during high repetition rate laser operation because of damage to the kaleidoscope. Thus the actual throughput used for wafer processing ranged from 50-60% for both lenses and kaleidoscope (the best value expected would be 73%).

The first quarterly report showed beam profiles of the raw excimer laser output which exhibited undesirable intensity spikes and non-uniformity. As demonstrated by the reticon profile shown in Fig. 2-2, improved homogeneity is achieved in the output of the kaleidoscope, reducing intensity fluctuations to the $\pm 10\%$ level and creating a very sharp intensity drop-off near the edges (compare to the raw beam profile shown in Fig. 2-3). It should be noted that the profile of Fig. 2-2 was the actual beam used in processing Batch 22. Unfortunately, the laser energy density used in Batch 22 was below the threshold for good junction formation. Later, improvements of the edge drop-off rate and squareness were found when the work surface or the reticon sensor surface was more carefully positioned with respect to the plane of best focus. The kaleidoscope proved quite adequate to homogenize the laser output beam.

As noted above, major damage to the kaleidoscope was observed when the beam was focused too near the front surface of the kaleidoscope. One kaleidoscope was fractured, and a second one exhibited small cracks and bubbles at the input end of the kaleidoscope, indicating light absorption leading to thermal fracture and melting of the glass. Three strategies have been implemented to overcome these difficulties: lowering the repetition rate of the laser to reduce thermal loading; moving the focus of the input lens further from the front surface of the kaleidoscope (with about 10% loss of intensity throughput); and taking care to keep the input end of the kaleidoscope clean. The third kaleidoscope has been operating satisfactorily for several weeks, and the two damaged kaleidoscopes have been repaired.

The necessity of lowering the laser repetition rate to assure survival of the kaleidoscope requires that the table speed be reduced appropriately. Previously the control program required user determination and entry of table speed. Since the table speed is controlled by a very non-linear potentiometer, accurate determination of this parameter was time control. Consequently, this operation has now been placed under computer control. The computer uses the given row length and software timed length between indexing and completed pulses to determine the table speed to an accuracy of about 0.1%. This value is then used to determine laser repetition rate.

During the quarter the propagation of the excimer beam through the kaleidoscope and complete lens system was studied using a ray trace code. The purpose of this study is to determine the expected beam uniformity and its dependence on lens design and demagnification. This code was specifically written to allow

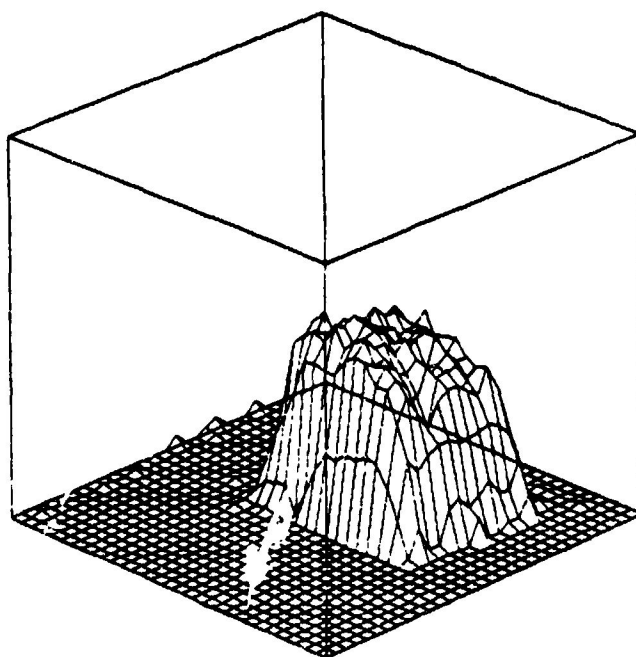


Fig. 2-2. Beam profile after kaleidoscope homogenization.

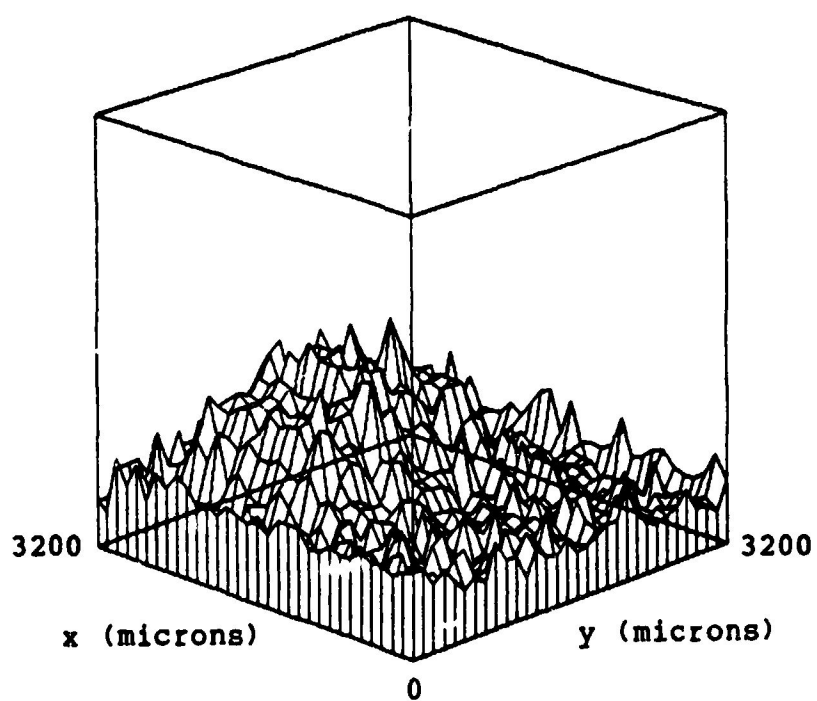


Fig. 2-3. Output beam with no external aperture.

entire planes of rays to be propagated through the optical system in three dimensions. An additional feature of this code included the ability to output spot diagrams of the beam at user-selected planes in the optical system. These diagrams proved useful in evaluating optical distortion, spot size, and distribution of rays in the plane. Special interest was centered on understanding the accuracy required to position the wafer surface relative to the objective lens used for reimaging the kaleidoscope output.

The ray trace algorithm uses a module which creates a set of equally spaced rays whose divergence is specified. The divergence may be different in the two orthogonal planes. The transverse extent of the input beam and its divergence are chosen to match the experimentally determined values. A particular ray at a given object location is assumed to diverge as a symmetric pencil of four rays. These assumptions were found to give focused spot sizes that agreed closely with experimentally determined values, whereas modeling of the beam as a point source with the same divergence produced spots that were much smaller than those observed experimentally. However, the actual ray distribution within a given plane will not be accurately represented because only four rays are used for each object point. The limit of four rays was chosen to minimize computational expense.

Three cases of interest were modeled using the code. The position of the optical components in each of these cases is shown in Fig. 2-4. Case 1 is the optical set-up for performing the annealing required to form a back surface field (BSF). The rather high energy densities required a 2:1 demagnification of the kaleidoscope output. Experimentally, it was known that the imaging in this case was somewhat unsatisfactory. The spot diagrams showing the beam at the kaleidoscope input, the kaleidoscope output, and the output near the plane of best geometric image are shown in Figs. 2-5 - 2-7. (The empty regions shown in Fig. 2-5 are a result of the fact that only four rays with maximum angular divergence were traced for each object point.) The axial position of best focus was determined by examination of several planes spaced 0.5 mm apart near the paraxial focus. Figure 2-4 shows the output at the kaleidoscope output plane that was used as the input for the three objective lens set-ups shown in Fig. 2-4. One notes the characteristic pattern that gives the kaleidoscope its name.

The input beam was modeled as a uniform distribution of rays in the object plane. This is contrary to known experimental conditions in which the beam is hottest in the center. When the rays are approximately weighted in a Gaussian fashion, the energy distribution is observed to be significantly flattened compared to the peaked input distribution, just as is observed experimentally. Physically this occurs due to the fact that marginal rays emerge, on average, near the optic axis, while rays near the center of the beam emerge farther from the center.

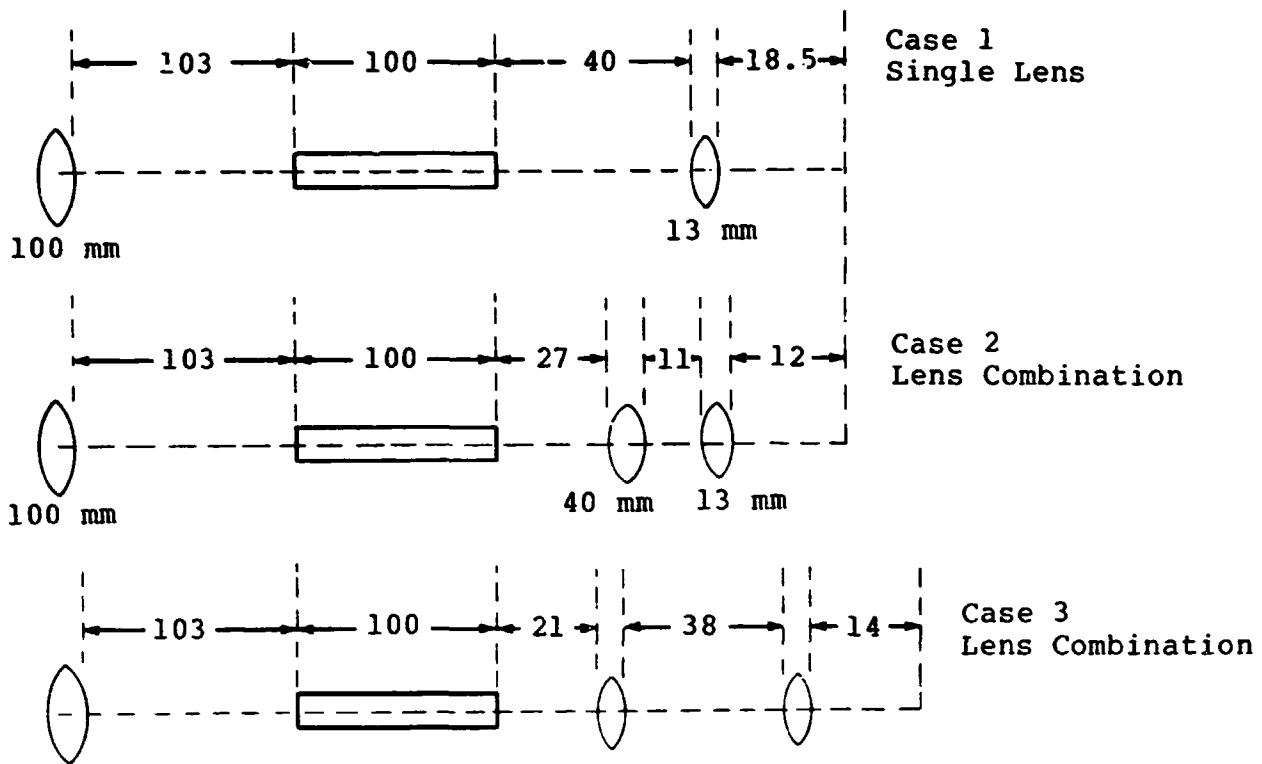


Fig. 2-4. Optical systems studied by ray tracing.

Not surprisingly, it was found that better homogenization results when the input beam has a significant inherent angular divergence. Since the small excimer laser has a 4-5 mrad half angle of divergence, the kaleidoscope technique is well suited to homogenize the beam. The drawback of the large angular divergence of the beam is the lack of focusability (see Fig. 2-5) which requires that the kaleidoscope front face be placed quite close to the focus of the input lens. The ray trace code showed that a significant number of rays are lost from the corners of the beam if the face is positioned more than 8 mm from the focal plane.

Figure 2-7 shows the spot diagram at the image plane for the case of a single 13 mm focal length lens. It can be seen that a significant number of rays fail to be collected within the main dark square measuring 0.8x0.8 mm (2:1 size reduction). By analogy with the usual geometric minimum blur circle, this might be called a smallest blur square. Some pinhole distortion is also noted at the spot boundary. The failure to adequately collect the marginal rays would be expected to be improved significantly by substituting the single lens with an equivalent two lens (Petzval type) combination. The best spacing between the two lenses was tested using the ray trace code. For each case several planes near the predicted paraxial image plane were plotted. The object-to-image distance for each case was based on the desired 2:1 size reduction. The two extreme cases of the

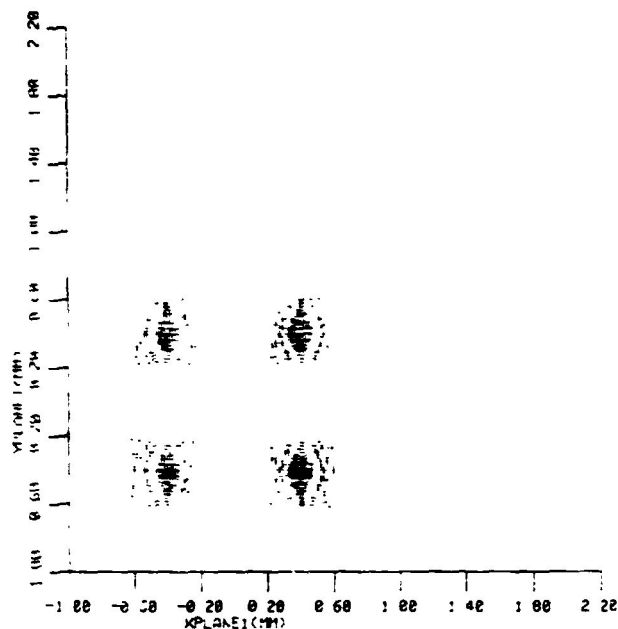


Fig. 2-5. Spot diagram at front surface of kaleidoscope for a beam with 4 mrad angular divergence.

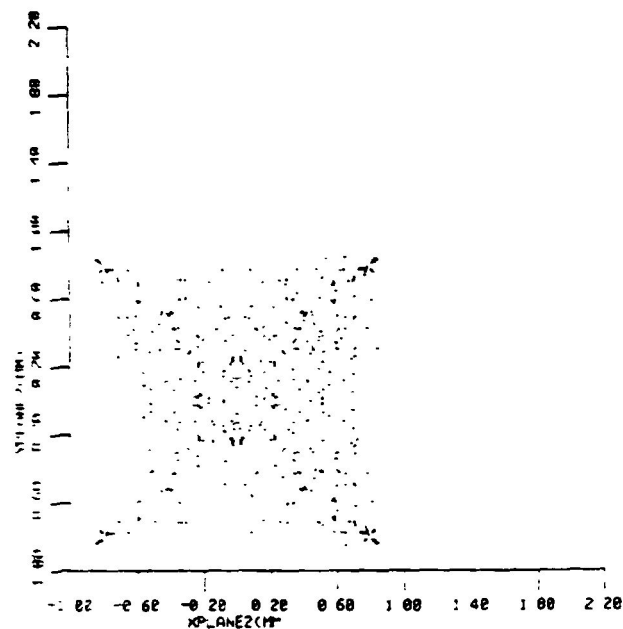


Fig. 2-6. Spot diagram at kaleidoscope exit plane for a beam with 4 mrad angular divergence.

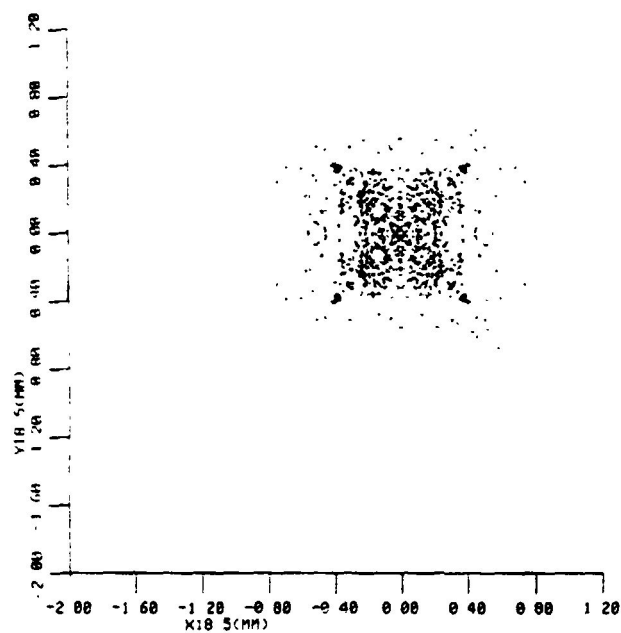


Fig. 2-7. Case 1: Single 13 mm lens, 2:1 reduction in size.

lens spacing of 0 and 40 mm were tested first. The former case showed only fair performance for this system and was not studied further.

Figure 2-8 shows the results obtained at a position of 14 mm from the final surface for Case 2 (see Fig. 2-1). In contrast to the single lens case, all rays except a few in the corners are reimaged within the desired spot area. The lens positions for Case 2 were chosen to give a lens combination whose equivalent focal length was 13 mm and whose secondary principal plane was approximately 3 mm from the front surface of the second lens. An additional advantage of the lens combination is the fact that the wafer surface may be displaced ± 0.5 mm without significant degradation of image quality. This is an improvement on the single lens case.

Figure 2-9 shows the image plane results for Case 3 (Fig. 2-4). The image is not as sharp as in Case 2 and has less positioning tolerance. However, the blur square size is improved over that of a single lens and so more of the total energy of the beam will hit the correct area on the wafer positioned at this location.

The question of the optimum edge drop-off rate for laser annealing has not been unequivocally resolved, however the current data suggest that the best cell efficiency has been obtained with sharp edge definition. Figure 2-10 is a reticon profile exhibiting the sharp edge drop-off (< 100 microns) found (experimentally) near the best focus. Also of interest in this figure is the well-defined plateau region which contains nearly all of the pulse energy. The ray trace studies indicate that movement of the wafer plane more than 0.5 mm in either direction results in loss of this sharpness if only a single lens is used. Use of lens combination Case 2 improves the focus tolerance.

2.1.3 Laser Annealing of Ion Implanted Wafers

Five groups (B16-B20) of wafers were laser annealed using the large laser, followed by 14 groups (B21-B29) of wafers that were annealed using the small laser with the beam homogenizer. Conditions for these processing experiments are listed in Tables 2-1 and 2-2.

After annealing, wafers from Batch 18 showed slight surface damage in some areas, indicating a threshold for damage of about 2.0 J/cm^2 when using the large laser and a 90 nsec pulse duration. In the case of the small laser, with a 30 nsec pulse duration, damage was observed on the surface of the wafers at about 1.5 J/cm^2 , especially at the edges of the spot. One factor affecting the damage threshold is the laser pulse shape. The damage threshold was lower (about 1.2 J/cm^2) for the pulse shape shown in Fig. 2-11a, whereas it was about 1.5 J/cm^2 for the laser pulse shape of Fig. 2-11b. The high intensity late in the pulse of Fig. 2-11a may produce excessive vaporization and surface damage.

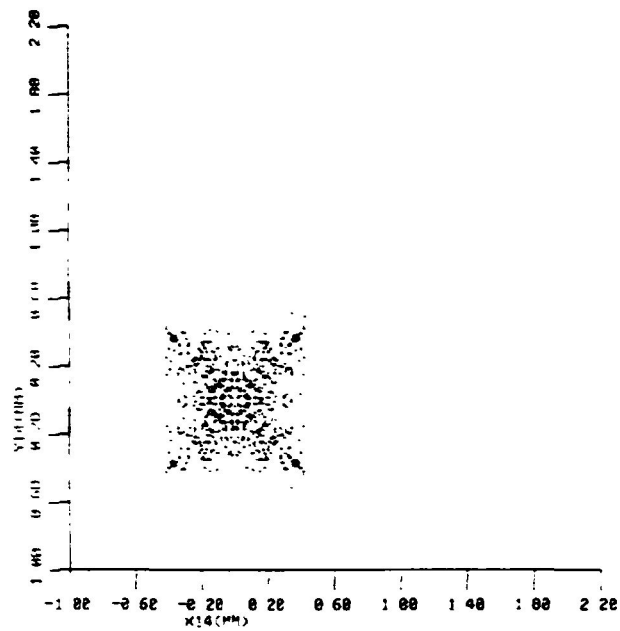


Fig. 2-8. Case 2: Results obtained by using two biconvex lenses with a combination effective focal length of 13 mm.

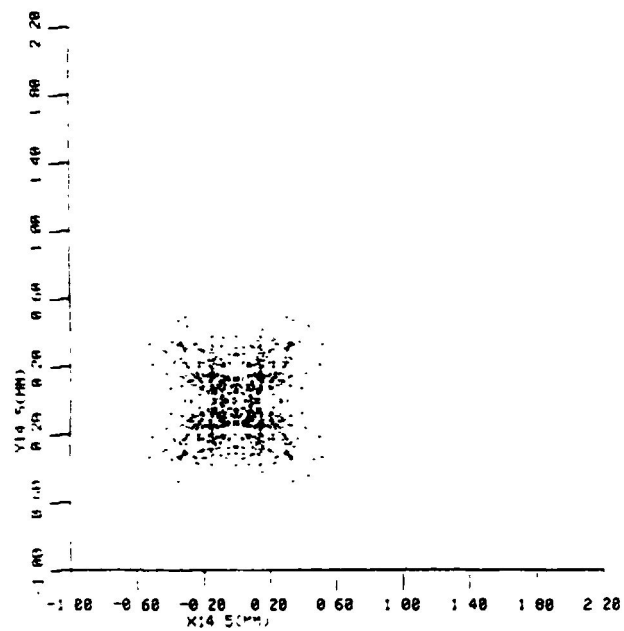


Fig. 2-9. Case 3: Spot diagram at image plane.

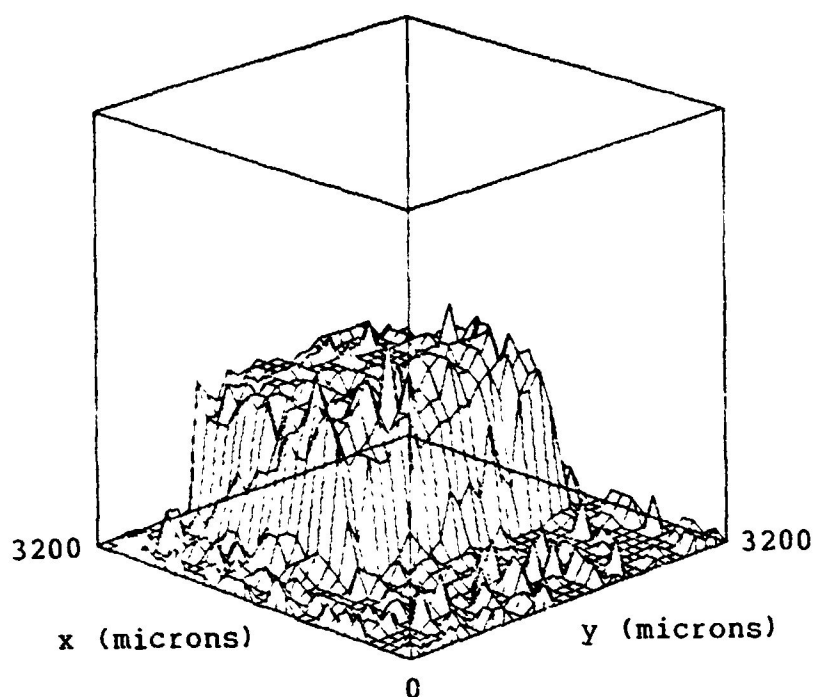


Fig. 2-10. Demonstration of edge fall-off of laser spot at wafer near best focus with single lens imaging.

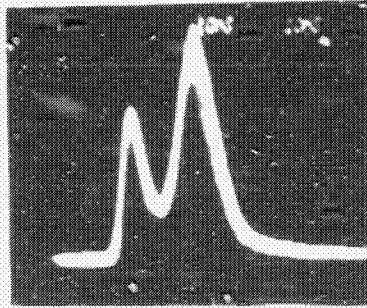
Table 2-1. Large laser (Lucy) annealing parameters. Pulse duration 90 nanoseconds, wafers doped by 5 keV ion implant except as noted.

Laser Energy (mJ)	Spot Size (mmxmm)	Average Energy Density (J/cm ²)	Spot Interval (mmxmm)	Overlap (%)	Remarks
Batch 16: 2 wafers					
1140	9.6x8.3	1.45	8.4x7.2	12	
Batch 17: 2 wafers					
1020	8.9x7.5	1.55	8.0x6.6	12	
Batch 18: 1 wafer					
1000	7.5x6.5	2.0	6.4x5.7	12	
Batch 19: 1 wafer					
1080	9.0x8.0	1.5	8.0x7.0	12	1 keV implant
Batch 20: 2 wafers					
1000	8.0x6.9	1.8	7.0x6.1	12	CVD doped
940	"	1.7	"	"	

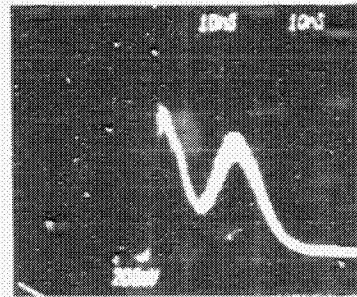
Table 2-2. Small laser (Exci-Lite) annealing parameters. Pulse duration 30 nanoseconds.

Laser Energy (mJ)	Spot Size (mmxmm)	Average Energy Density (J/cm ²)	Table Speed (cm/sec)	Spot Interval (mmxmm)	Over-lap (%)	Remarks
Batch 21: 1 p+ n n+ wafer, front by ion implant at 10 keV, 1x10 ¹⁵ , back at 50 keV, 10x10 ¹⁵ atom/cm ²						
13	1.3x1.2	0.8	2.5	0.9x0.7	30	Front; spots too large
"	1.1x0.9	1.3	"	0.9x0.35	50	Back; spots too large
Batch 22: 4 p-type wafers, 31p+ implant at 5 keV, 2.5x10 ¹⁵ atom/cm ²						
13	0.8x0.8	2.0	1.2	0.64x0.64	20	Kaleidoscope face damage (2 wafers)
"	"	"	"	"	"	"
14	0.95x0.9	1.6	1.2	0.75x0.7	20*	New kaleidoscope; slight damage on wafers
"	"	"	"	0.48x0.45	50	"
Batch 23: 3 wafers: first n-type, 11B+ implant at 5 keV, 2.5x10 ¹⁵ atom/cm ² ; others p-type, 31p+, 5 keV, 5 and 1x10 ¹⁵						
10	0.9x0.85	1.3	1.2	0.40x0.38	50	Low laser reliability; high intensity at end of pulse; no cells made
"	"	"	"	"	"	
"	1.0x0.95	1.1	"	0.45x0.42	"	"
Batch 24: 3 p-type wafers, 31p+ implant at 5 keV, 1, 2.5, 5x10 ¹⁵ atom/cm ²						
12	0.95x0.9	1.4	0.8	0.45x0.42	50	Good laser reliability and pulse shape
"	"	"	"	"	"	
"	"	"	"	"	"	"
Batch 25: 1 n-type wafer, 11B+ implant at 5 keV, 2.5x10 ¹⁵ atom/cm ²						
13	0.95x0.9	1.52	0.8	0.45x0.43	50	To Batch 27
Batch 26: 3 p-type wafers, 31p+ implant at 5 keV, 1, 2, 5x10 ¹⁵ atom/cm ²						
15.5	1.05x1.0	1.45	0.8	0.53x0.5	50	New cleaning method
Batch 27: 1 wafer, p+ n n+ front from 25, n+ spun-on, annealed as below						
13.5	0.7x0.7	2.7	0.7	0.35x0.33	50	Focus not sharp
Batch 28: 3 p-type wafers, 31p+ implant at 5 keV, 1, 2.5, 5x10 ¹⁵ atom/cm ²						
14	1.0x0.95	1.45	1.0	0.48x0.45	50	Beam less uniform than Batch 26
Batch 29: 1 p+ n n+ wafer, 11B+ implant at 5 keV, 2.5x10 ¹⁵ atom/cm ² on front; n+ spun on back						
15	1.05x1.0	1.43	0.8	0.40x0.38	60	Fuzzy at spot edges

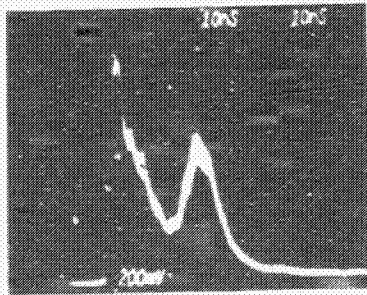
*ion implant at 5 keV, 1x10¹⁵ atom/cm²



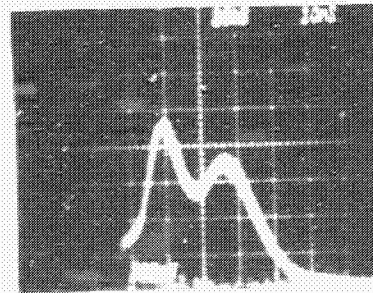
a. Batch 23.
Low damage threshold.
 1.2 J/cm^2



b. Batch 24.
Higher damage threshold.
 1.5 J/cm^2



c. Batch 26.



d. Batch 33.
After modification
of pulse forming line.

Fig. 2-11. Excimer laser pulse waveforms.

Good solar cell results were obtained from the wafers processed in Batch 24. Just prior to this test the laser had been disassembled to determine the reason for excessive shot-to-shot variability. The screen electrode was smoothed and the laser mirrors were cleaned. In addition, the resistor in series with the corona bar was reduced, thereby increasing the strength of the UV preionization and improving the reproducibility of the electrical discharge in the laser gas.

Good solar cell results also were obtained from the wafers processed in Batch 26, even though there were slight residual damage marks on the wafer surface at the edges of each laser spot. The laser pulse waveform used in these experiments is shown in Fig. 2-11c. The overall pulse duration is 30 nsec, with the higher intensity during the early part of the pulse. The laser spot was sharply focused on the wafer, was square, and the overlap was set carefully to 50% in both directions. The highest cell efficiency was obtained with 5 keV, 2.5×10^{15} cm⁻² phosphorus ion implant energy and dose using wafers that had been cleaned just three days prior to the laser processing.

Following Batch 27, a careful study was made of the laser intensity distribution, both spatial and temporal, at the exit of the kaleidoscope and also at the location of the wafer surface. Particularly close attention was directed at the edges of the spot to see if the intensity or pulse shape was altered in a way that would induce surface damage specifically at the edge of each spot. A fast response photodiode recorded the laser intensity from the portion of the laser beam transmitted through a 25 micron pinhole, mounted on an x-y-z micropositioning assembly. In addition, the surface damage on 5 keV ion implanted wafers was examined as a function of the laser parameters such as energy density, laser pulse waveform, and edge sharpness of the spot on the wafer. As a result of the improved pulse shape (such as that shown in Fig. 2-11d), the following observations were made:

1. No indications of laser intensity or pulse waveform changes near the edges of the spot were seen other than the expected falloff in intensity at the edges.
2. The top and bottom edges of the spot showed more abrupt intensity changes than did the sides. The damage to the wafer was more severe at the top and bottom edges. The laser output has greater beam spread up and down, filling the kaleidoscope better and making the intensity gradient sharper at the output of the kaleidoscope.
3. Surface damage appeared to be essentially the same whether single spots were used, or multiple spots with 50% overlap.
4. By significantly defocusing the spot on the wafer it was possible to eliminate the edge damage that was observed. With higher laser energy density in the central portion of

the spot (1.6 to 1.7 J/cm²), a speckle pattern of surface damage was seen, but with no edge damage noticeable.

5. Wafers with higher ion implant dose showed greater susceptibility to damage than wafers with low dose. Any surface film on the wafer reduced the damage threshold.
6. Slight luminosity is seen on the wafer surface as the laser spot impinges when the laboratory is darkened. The luminosity may be due to vaporization of Si, P, or a thin residual surface layer such as SiO₂.

2.1.4 Optical Transport and Beam Shaping for Surface Passivation and Metallization Process Steps

The surface passivation and metallization experiments will be carried out inside a vacuum tight chamber currently being fabricated. The excimer output beam must be transported to this chamber and focused with minimal loss and distortion. Due to the short wavelengths (193 nm) involved the beam will be transported inside a nitrogen or inert gas filled light tube. A straight line optical path is preferred to avoid losses on bending mirrors.

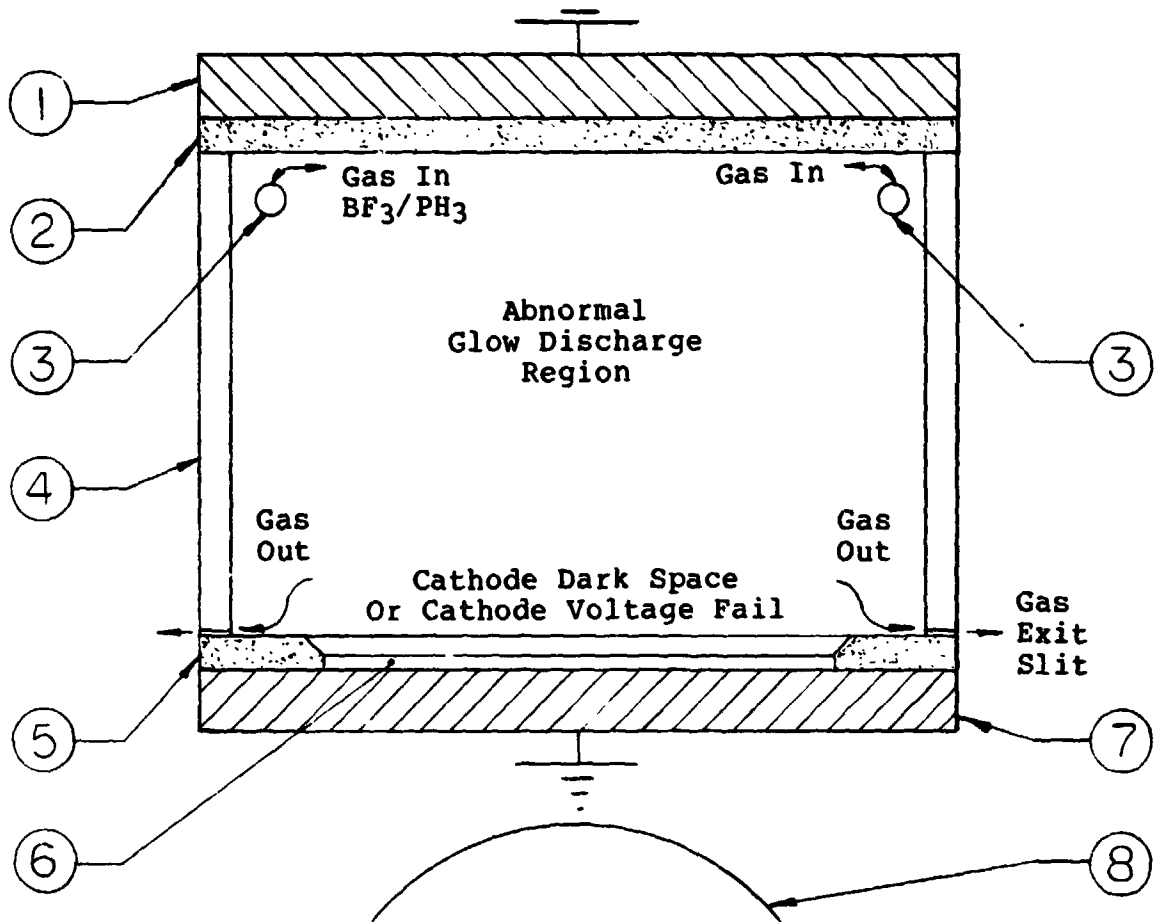
For the metallization step a thin line of light focused on the wafer surface is required. Such a condition may be achieved using a cylindrical lens positioned close to the entrance window of the gas cell. All transmissive optics must be high grade suprasil or dynasil 1000. The line of light will be 10 to 15 mm long. Mechanical translation of the lens and mirror assembly will allow complete cell coverage of a metallization pattern. Individual lines will be written by mechanical translation of the lens and mirror assembly after a suitable empirically determined exposure time.

For these experiments a good optical quality beam is required. The necessary unstable resonator optics for the small excimer laser are being ordered.

2.2 ION IMPLANTATION

2.2.1 Glow Discharge Ion Implantation

The glow discharge ion implantation design concept is complete. Detailed design and fabrication are under way. The design concept includes a vacuum system for safety and convenience, as shown schematically in Fig. 2-12. The anode backing plate is a 17"x1/2"x6" water-cooled copper plate which is part of the vacuum system. Since hazardous gases will be used, safety features are essential. These include a vented gas cabinet for three source gas bottles, an interlocked gas distribution system, a vented enclosure around the system, and a gas scrubber for the pump exhaust.



1. Anode backing plate, copper (17"x1/2"x6")
water cooled
2. Silicon anode + potential
3. Gas manifold, quartz
4. Plasma containment envelope, quartz
5. Silicon sample holding frame
6. Sample, 4"x4" Si wafer, 2 each
7. Cathode, ground potential
8. Sample heater

Fig. 2-12. Schematic of glow discharge implantation chamber.

Silicon slabs from a Cz ingot are being fabricated to form the anode. A quartz plasma containment envelope will be fixed to the anode to form the walls of the reaction vessel. The envelope, along with a symmetric gas distribution manifold, is being fabricated (Fig. 2-13). The samples to be implanted will be spaced 4" apart on the sample holding frame and will face the anode. All surfaces exposed to the plasma will be silicon or quartz to avoid contamination. The sample holding frame will be held in an aluminum cathode which can be heated with an existing graphite cloth heater.

2.2.2 Ion Gun Implantation

A new, unique low-energy, 500 eV ion gun has been developed by Green et al. of the University of Illinois Coordinated Science Lab (private communication). Six 1"x1" samples of Cz silicon will be implanted with arsenic for evaluation of this technique.

2.2.3 Ion Milling Implantation

Low keV ion implant was reported possibly done by the ion milling technique at IICO (Santa Clara) using Kaufman Milling Source MTL20. Samples were sent for 1 keV PF_5 implant with fluence of 5×10^{15} atoms/cm².

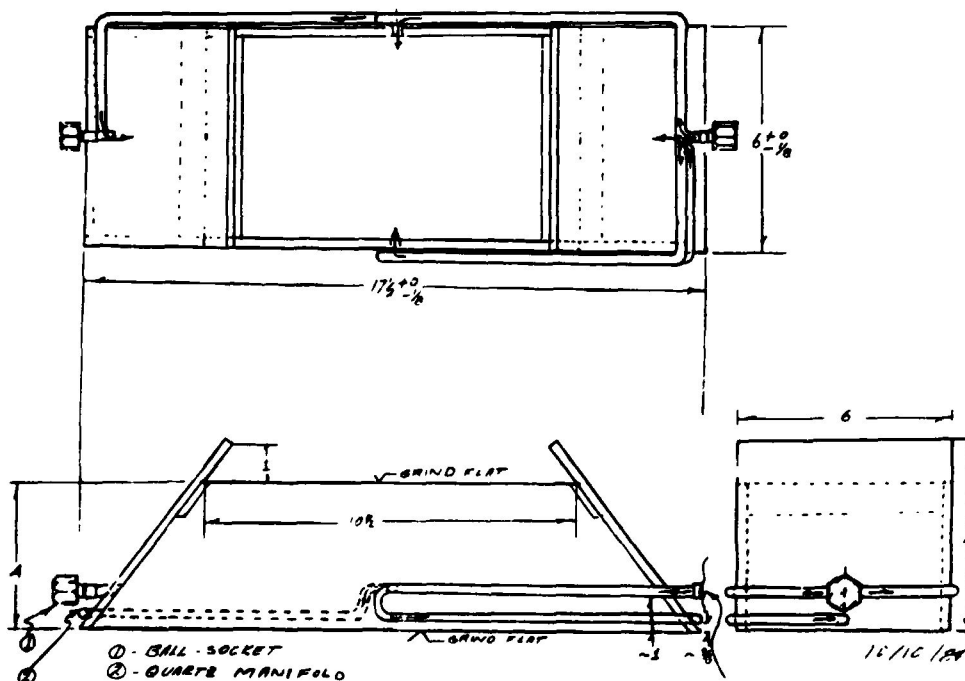


Fig. 2-13. Quartz envelope inside implantation chamber.

2.3 LASER-ASSISTED CVD EQUIPMENT

A gas distribution system is being assembled for laser-assisted metal deposition and laser-enhanced CVD experiments. A gas cabinet for storage and delivery of up to three hazardous gases has been specified and ordered from Matheson Gas Products. Figure 2-14 shows a schematic for two of the gases; the third gas will be trimethyl aluminum delivered from a Schumacher bubbler.

A flow measurement and mixing manifold together with the control panel are being designed and will be built into the gas cabinet.

The remaining parts of the system to be designed and built are the pumping system, sample heater, and gas scrubber.

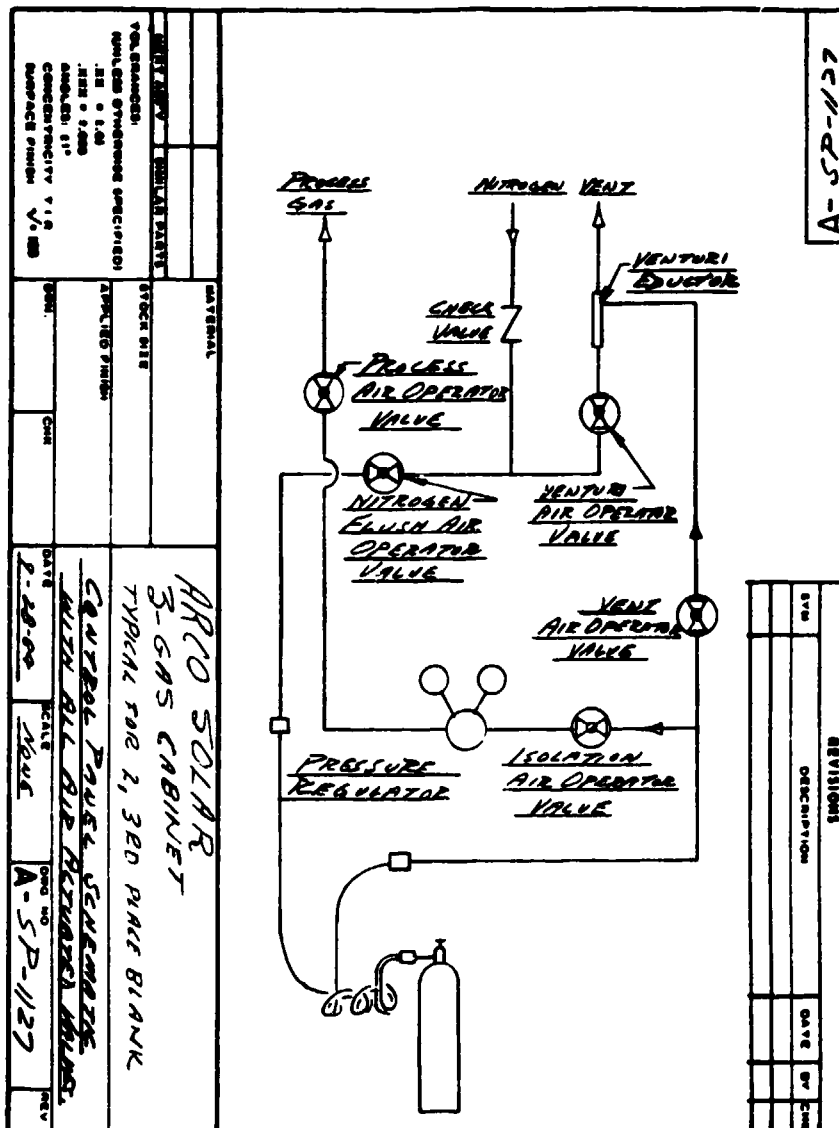


Fig. 2-14. Gas cabinet schematic.

SECTION 3.0 EXPERIMENTAL

Results from the fourth month of effort demonstrated that the higher power laser (4 J output) with the larger beam size ($\approx 1 \text{ cm}^2$) was capable of producing 9.6% Cz cells without optimizing the beam homogeneity, gridline pattern, and BSF. However, the slow repetitive pulse rate of this laser (1 pulse per 2 minutes) made it impractical for extensive experimentation or production consideration. During the remainder of the quarter, effort was devoted to developing the smaller laser which has a repetition rate as fast as 25 Hz. The faster process speed enables more experiments to be performed.

3.1 CELL PROCESSING BY LARGE LASER, "LUCY"

Three experiments were conducted. Material was p-type (0.7 ohm-cm) Cz, ion implanted with 31p^+ at 5 keV of fluence 1×10^{15} atoms/cm². Details of the laser and x-y table operating parameters are listed in Table 2-1; electrical performance of the cells is presented in Table 3-1.

With such a wide range of laser energy density (from 1.45 J/cm² to 2.0 J/cm²), there was little difference in cell efficiency, except for several bad cells (B16 #3, B18 #3). However, the data did show a trend of V_{oc} improvement as annealing energy density increased, suggesting more lattice damage removal with higher energy density. A wafer from B18 showed slight surface damage in some areas, indicating a threshold for damage of about 2.0 J/cm² for 80 nsec pulse duration.

The overall V_{oc} was lower than furnace-diffused control samples by about 10 mV. This could be due to surface recombination at the overlap boundaries and also the low ion implant dosage that produced a weak electrical field at the junction.

Before the large laser (Lucy) was idled, two more experiments (B19, B20) were conducted as base-line processing on a Cz wafer (p-type 0.7 ohm-cm) that had been ion implanted at 1 keV (2×10^{15} atoms/cm²) and 5 keV (2.5×10^{15} atoms/cm²) respectively. The 1 keV ion implant was performed by IICO at Santa Clara. The ion beam was first accelerated to 25 keV and decelerated by increasing the target distance. Metallization involved 18 evaporated gridlines with 9% shadowing. Data are summarized in Table 3-2. Also included are results from control cells processed by thermal deposition-diffusion from the same batch of Cz starting material.

The average J_{sc} for 1 keV ion implanted cells (B19) was almost 7% (1.4 mA/cm²) higher than 5 keV implants (B20) due to shallower junction characteristics. However, because of the low surface dopant concentration, the V_{oc} of the 1 keV samples was

Table 3-1. Electrical performance of "Lucy" processed Cz cells. No AR coating. Implant energy = 5 keV; ion fluence = 1×10^{15} atom/cm². Cells measured at AM1.5, 25°C.

a. Laser energy density = 1.45 J/cm²; overlap = 12%.

Cell ID	J _{sc} (mA/cm ²)	V _{oc} (V)	FF (%)	Eff (%)
B16				
#1	21.16	0.576	74.58	9.10
#2	21.57	0.578	76.94	9.60
#3	19.62	0.571	76.01	8.52
#4	21.61	0.574	75.08	9.32

b. Laser energy density = 1.55 J/cm²; overlap = 12%.

Cell ID	J _{sc} (mA/cm ²)	V _{oc} (V)	FF (%)	Eff (%)
B17				
#1	20.70	0.577	76.14	9.10
#2	21.03	0.578	74.41	9.04
#3	21.64	0.580	74.53	9.36
#4	21.35	0.579	76.16	9.41

c. Laser energy density = 2.0 J/cm²; overlap = 12%.

Cell ID	J _{sc} (mA/cm ²)	V _{oc} (V)	FF (%)	Eff (%)
B18				
#1	21.37	0.587	74.49	9.35
#2	21.02	0.588	76.79	9.49
#3	20.83	0.553	40.99	4.72
#4	21.08	0.587	76.87	9.52

Table 3-2. Laser annealing by large laser on ion-implanted Cz wafers.

- a. Implant energy = 1 keV; ion fluence = 2×10^{15} atom/cm²; energy density = 1.5 J/cm²; overlap = 12%.

Cell ID	Sheet Rho (ohm/sq)	J _{sc} (mA/cm ²)	V _{oc} (V)	FF (%)	Eff (%)
B19					
#1	>100	20.66	0.537	73.20	8.12
#2	"	21.77	0.525	70.43	8.05
#3	"	21.61	0.524	70.29	7.96
#4	"	21.59	0.531	72.08	8.26
#5	"	21.16	0.509	70.04	7.54
#6	"	21.53	0.544	69.29	8.12

- b. Implant energy = 5 keV; ion fluence = 2.5×10^{15} atom/cm²; energy density = 1.8 J/cm²; overlap = 12%.

Cell ID	Sheet Rho (ohm/sq)	J _{sc} (mA/cm ²)	V _{oc} (V)	FF (%)	Eff (%)
B20					
#1	35-45	19.54	0.582	70.30	8.00
#2	"	20.21	0.576	71.14	8.28
#3	"	20.50	0.580	69.82	8.30
#4	"	20.19	0.577	67.97	7.93

- c. Control cells (R52-B19) processed by thermal deposition-diffusion from the same starting material, p-type 0.7 ohm-cm.

Cell ID	Sheet Rho (ohm/sq)	J _{sc} (mA/cm ²)	V _{oc} (V)	FF (%)	Eff (%)
R52-B19					
#1	- - - Shunted - - -				
#2	50-60	21.30	0.594	77.53	9.81
#3	"	21.85	0.595	76.83	9.98
#4	"	21.86	0.595	76.38	9.91

substantially lower by 8.8%. The gain in J_{sc} while V_{oc} was reduced, and vice versa in these two samples, equalized their final efficiency to 8% on average, while the control cells averaged 9.9% (omitting the obviously shunted cell). Results suggest that the shallow junction formed by the 1 keV ion implant with sufficient surface dopant concentration should be able to yield J_{sc} and V_{oc} as high as the thermally diffused cell. Theoretically, higher V_{oc} would be obtained only if the laser homogeneity could be improved to allow 5% or less overlap. Decreasing the overlap without laser homogeneity improvement would have an adverse result due to nonuniform annealing. For nonuniform beams, a higher overlap ratio could yield better results than a lower overlap ratio.

3.2 CELL PROCESSING BY SMALL LASER, "EXCI-LITE 1"

3.2.1 p-Type Substrate With $31p^+$ Ion Implant Dopant

After the installation of kaleidoscopes, the first experiment with the small laser, Exci-Lite 1, was to redefine the energy density range which is highly dependent on pulse shape and pulse duration. The melt penetration depth for 30 nsec of the Exci-Lite laser could be almost 50% deeper than 90 nsec of Lucy's at the same laser energy density (R. Young et al., 1983). The threshold annealing energy density, therefore, is different for these two different lasers. Due to the difference in beam uniformity, beam overlap percentage is also a critical parameter. Detailed annealing parameters are listed in Table 2-2.

The experiment (B22) with Exci-Lite started by using the same Cz material and ion implantation (5 keV, 2.5×10^{15} atoms/cm²) as for B19 and B20 that were processed by Lucy. Laser energy density was set at 1.6 J/cm² with 50% and 20% overlap, respectively, and 2.0 J/cm² with 20% overlap. For comparison, samples that were 5 keV ion implanted at 1×10^{15} atoms/cm² dosage were also annealed at 1.6 J/cm² with 20% overlap. Such ion implanted material had been demonstrated to yield cells with efficiencies >9.5% in three consecutive runs (B16, B17, B18) processed by the larger laser (see Section 3.1).

As indicated by Table 3-3, results of the whole experiment (B22) were poor. Even the 1×10^{15} atoms/cm² samples (B22-V) were degraded in both V_{oc} and fill factor compared with previous runs reported earlier.

Comparing the electrical performance of B22-II (50% overlap) with B22-III (20% overlap), both annealed at 1.6 J/cm² energy density, it was clear that the low V_{oc} (0.55 V) of the latter (20% overlap) was due to incomplete surface annealing because of the beam's inhomogeneity. As overlap was increased to 50% (B22-II), the V_{oc} was improved to 0.583 V, similar to previous results obtained from the large laser. The poor fill factor was believed to be due to surface contamination as revealed by optical photos (Fig. 3-1).

Table 3-3. Laser annealing by improved small laser on ion-implanted Cz wafers. Implant energy = 5 keV.

- a. Ion fluence = 2.5×10^{15} atom/cm²; energy density = 1.6 J/cm²; overlap = 50%.

Cell ID	Sheet Rho (ohm/sq)	J _{sc} (mA/cm ²)	V _{oc} (V)	FF (%)	Eff (%)
B22-II					
#1	38-40	19.84	0.579	66.05	7.59
#2	"	19.76	0.587	70.97	8.24
#3	"	18.97	0.576	60.44	6.61
#4	"	20.22	0.583	70.43	8.31

- b. Ion fluence = 2.5×10^{15} atom/cm²; energy density = 1.6 J/cm²; overlap = 20%.

Cell ID	Sheet Rho (ohm/sq)	J _{sc} (mA/cm ²)	V _{oc} (V)	FF (%)	Eff (%)
B22-III					
#1	38-40	19.26	0.542	34.34	3.59
	"	20.07	0.557	46.23	5.17
	"	19.51	0.566	44.82	4.95
	"	19.09	0.541	34.62	3.57

- c. Ion fluence = 2.5×10^{15} atom/cm²; energy density = 2.0 J/cm²; overlap = 20%.

Cell ID	Sheet Rho (ohm/sq)	J _{sc} (mA/cm ²)	V _{oc} (V)	FF (%)	Eff (%)
B22-IV					
#1	>100	21.00	0.507	69.72	7.74
#2	"	22.06	0.493	65.84	7.71
#3	"	21.37	0.492	70.29	7.39
#4	"	20.03	0.458	48.77	4.48
#5	"	- - - Broken - - -			
#6	"	21.92	0.500	66.95	7.34
#7	"	20.39	0.457	51.58	4.80
#8	"	21.44	0.487	62.35	6.51

- d. Ion fluence = 1×10^{15} atom/cm²; energy density = 1.6 J/cm²; overlap = 20%.

Cell ID	Sheet Rho (ohm/sq)	J _{sc} (mA/cm ²)	V _{oc} (V)	FF (%)	Eff (%)
B22-V					
#1	92	20.49	0.577	93.48	8.68
#2	"	20.29	0.574	70.34	8.20
#3	"	20.71	0.578	67.15	8.04
#4	"	21.29	0.577	67.97	8.35

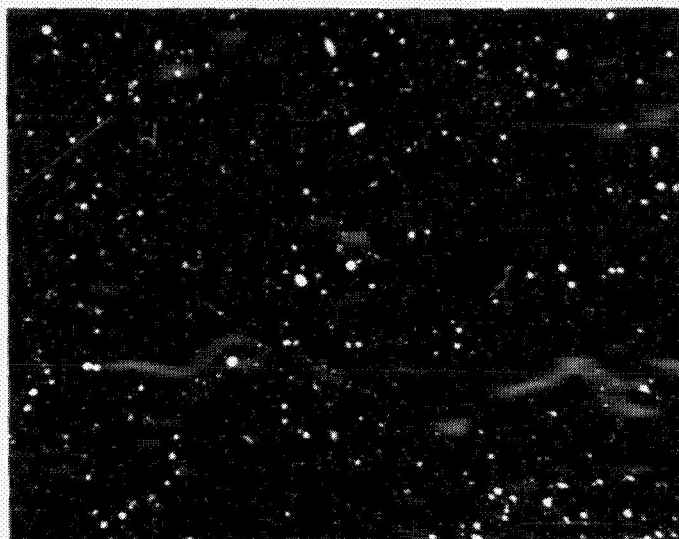


Fig. 3-1. Surface contamination.

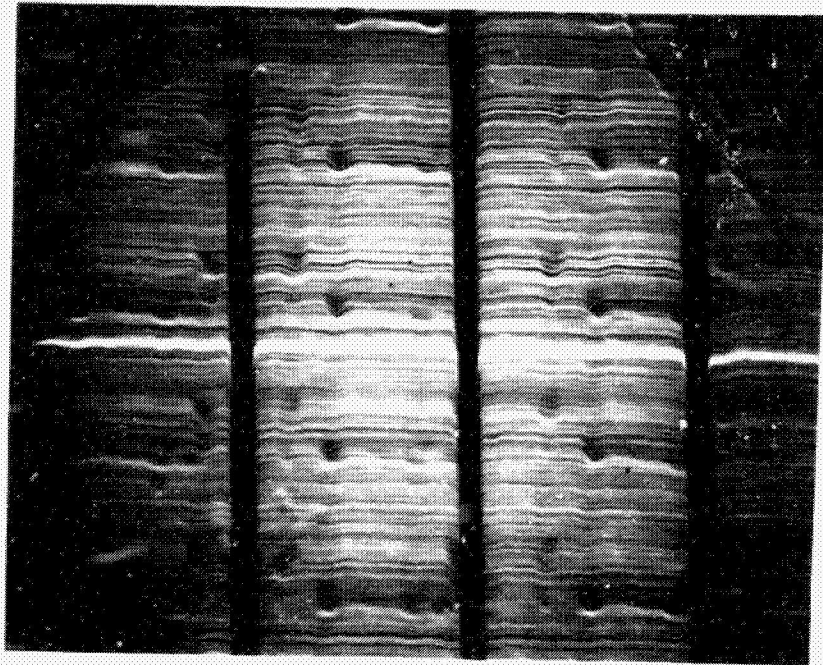
Incomplete surface annealing due to insufficient overlap was further demonstrated by increasing the energy density to 2.0 J/cm^2 (B22-IV) while keeping overlap to 20%. No further improvement in V_{oc} was obtained. Laser scanning (Fig. 3-2a) over the surface indicated current sink points along the overlap area, suggesting heavy damage due to localized overheating. A cell from this group had been preferentially etched with Secco etchant after metal contacts were removed. The optical photo revealed massive surface defects (Fig. 3-2b).

The results from B22 suggested that 20% overlap was not sufficient to compensate for beam nonuniformity. Also, even 1.6 J/cm^2 was too high at 30 nsec pulse (double peaks) duration to cause surface damage.

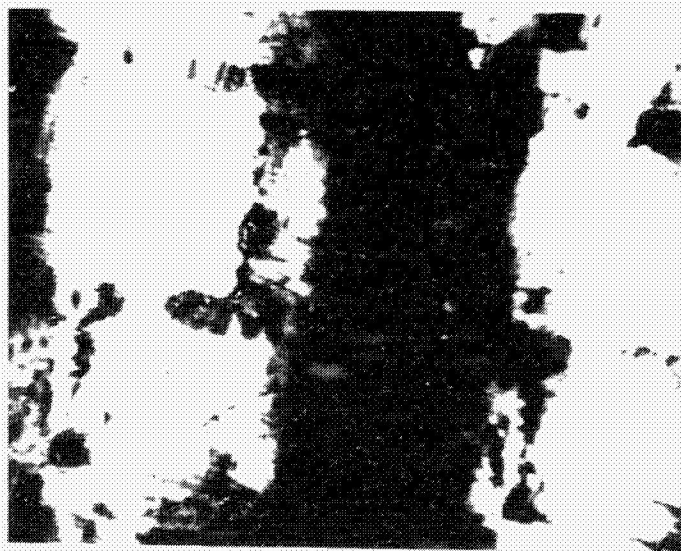
The next experiment, B23, was then conducted to study defects vs laser energy from 1.1 J/cm^2 to 1.3 J/cm^2 with 50% overlap. Samples were then Secco etched. Optical photos at 50x are presented in Fig. 3-3 while the laser parameters and the respective sheet resistivities are summarized in Table 3-4. Results suggest that 1.3 J/cm^2 with 50% overlap apparently produced the ideal range in sheet resistivity for dosages of 2.5×10^{15} to $5 \times 10^{15} \text{ atoms/cm}^2$, while the surface concentration was low for the $1 \times 10^{15} \text{ atoms/cm}^2$ dosage.

The degree of surface damage due to the imprint of the laser beam was apparently quite different for 1.1 J/cm^2 and 1.3 J/cm^2 (Fig. 3-3). Provided that the laser output and pulse shape were reproducible, the annealing threshold energy in optimizing dopant activation vs surface damage for the Exci-Lite small laser would be very close to 1.3 J/cm^2 with 50% overlap. Whether it can provide complete lattice damage removal caused by 5 keV $^{31}\text{P}^+$ ion implant is not certain at this stage.

ORIGINAL FACTOR
OF POOR QUALITY



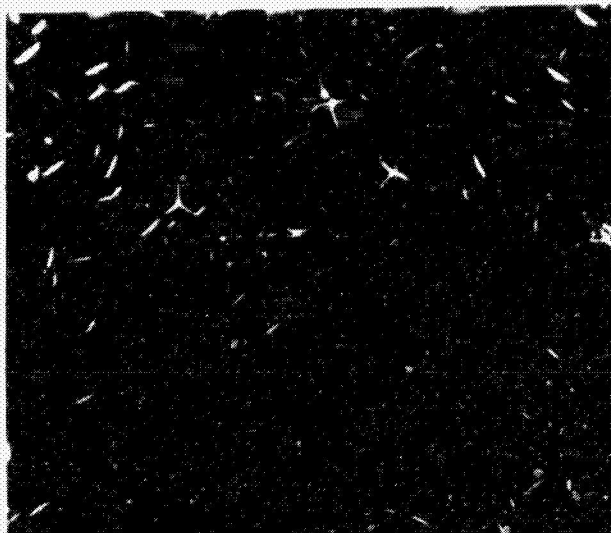
- a. 2.0 J/cm², 20% overlap laser annealed cell. Dark vertical lines are contact fingers. Dimpled structures are damaged areas along annealing directions, faintly observable.



- b. Surface appearance after preferential etch. Imprints of the laser beam are recognizable.

Fig. 3-2. Laser scan showing incomplete surface annealing.

ORIGINAL PAGE IS
OF POOR QUALITY



a. 1.3 J/cm^2



b. 1.3 J/cm^2



c. 1.1 J/cm^2

Fig. 3-3. Surface damage revealed by etching.

Table 3-4. Sheet resistivity of wafers. Implant energy = 5 keV; overlap = 50%.

Cell ID	Crystal Zoning	Base Resistivity (ohm-cm)	Ion Fluence $\times 10^{15}$ atom/cm ²	Laser Energy (J/cm ²)	Sheet Rho (ohm/sq)
B23					
-I	FZ	0.3	5	1.3	22-24
-II	Cz	0.7-0.9	2.5	1.3	52
-III	Cz	0.7-0.9	1	1.1	85-90

The surface damage that appeared on sample B23-I (Fig. 3-3a) was of a crystallographic type. Although the exact cause is not determined yet, it is possibly due to surface contamination. Such contaminants acted as nuclei for recrystallization during the melting-solidification process. Both epitaxial regrowth and free (no-constraint) recrystallization are clearly distinguishable by the (100) and (111) structures at such defects.

An experiment (B24) immediately following the test run was then conducted with 50% beam overlap at 1.4 J/cm² energy density. Material used included Cz (0.7 ohm-cm p-type) ion implanted at 5 keV with 1×10^{15} and 2.5×10^{15} atoms/cm² respectively, and FZ (0.3 ohm-cm, p-type) ion implanted at 5 keV with 5×10^{15} atoms/cm² fluence. Originally there were four wafers 2x2 cm in size prepared from each group. Some wafers were used for defect studies, leaving only seven pieces for final metallization. Results of electrical performance are summarized in Table 3-5.

While the average J_{sc} was in the same range as previous experiments, the fill factor was strikingly improved from 40-62% in previous experiments to over 74-78% in this run (B24). The V_{oc} was also increased to as high as 0.594 V (B24-II #3). The FZ sample in the same experiment had V_{oc} of 0.61 V. The higher V_{oc} obtained in the FZ sample was due to its lower base resistivity (0.3 ohm-cm vs 0.7 ohm-cm in Cz). The maximum cell efficiency from this experiment (B24) was 9.77% (B24-II #3). The large variations in fill factors among these cells are thought to be due to surface conditions already discussed (ref. Fig. 3-1).

Using information obtained from B23 and B24 that included laser energy density, overlap ratio, and surface conditions, a summary experiment (B26) was conducted. Material used consisted of Cz (0.7 ohm-cm) and FZ (0.3 ohm-cm). Wafers were cleaned by scrubbing in detergent, 10% HF acid etching, $H_2SO_4+H_2O_2$, HF acid etching, and finally soaking in HCl acid before deionized water rinsing. Although water spots were still present, their density was drastically decreased. Due to lack of adequate equipment for scrubbing, surface scratches were observed on some wafers. Ion

Table 3-5. Electrical performance of B24 cells. Implant energy = 5 keV; energy density = 1.4 J/cm²; overlap = 50%.

a. Cz cells. Ion fluence = 1×10^{15} atom/cm².

Cell ID	Sheet Rho (ohm/sq)	J _{sc} (mA/cm ²)	V _{oc} (V)	FF (%)	Eff (%)
B24-I					
#1	90	21.06	0.581	76.63	9.38
#2	"	21.26	0.581	75.80	9.50

b. Cz cells. Ion fluence = 2.5×10^{15} atom/cm².

Cell ID	Sheet Rho (ohm/sq)	J _{sc} (mA/cm ²)	V _{oc} (V)	FF (%)	Eff (%)
B24-II					
#1	46	20.88	0.593	78.10	9.66
#2	"	20.88	0.593	73.61	9.06
#3	"	21.26	0.594	77.40	9.77

c. FZ cells. Ion fluence = 5×10^{15} atom/cm².

Cell ID	Sheet Rho (ohm/sq)	J _{sc} (mA/cm ²)	V _{oc} (V)	FF (%)	Eff (%)
B24-III					
#1	23	21.49	0.611	73.63	9.67
#2	"	21.37	0.607	67.93	8.81

implant energy was 5 keV on both Cz and FZ wafers. The dosage for Cz was 1×10^{15} atoms/cm² and 2.5×10^{15} atoms/cm², and 5×10^{15} atoms/cm² for FZ material. The results are summarized in Table 3-6.

Cells processed from 5 keV ion implant with dosage 1×10^{15} atoms/cm² were slightly better than in the previous experiment (B24) in J_{sc} and fill factor. Cells from dosage 2.5×10^{15} atoms/cm², however, had obvious improvements in both J_{sc} and fill factor. While the increased J_{sc} is not immediately explainable, the improvement in fill factor is most likely due to surface cleanliness.

The maximum and minimum efficiency of group B26-2.5E is 10.22% and 10.08% respectively before AR, with 18 gridlines producing 9% shadowing. These cells were sent to ASEC for AR coating. The best cell (B26-2.5E #2) had an efficiency of almost 15.8%. The light and dark I-V curves of this cell are presented in Fig. 3-4; Fig. 3-5 shows the spectral response at AM1.5.

Results from the FZ material with ion fluence of 5×10^{15} atoms/cm², however, had a poor result in all respects. From this experiment, it is obvious that ion implant energy near 5 keV with fluence about 3×10^{15} atoms/cm² is capable of producing a high efficiency cell.

The experiment (B28) was repeated for the two Cz wafers (2"x2") with 2.5×10^{15} atoms/cm² fluence at the similar laser settings except slightly decreased in energy density from 1.5 J/cm² to 1.45 J/cm². Cells were processed utilizing photolithographic metallization techniques followed by AR coatings. Results are shown in Table 3-7.

Both J_{sc} and V_{oc} of this run were almost equal to the previous one. It was the fill factor that differed significantly and is believed to be due to either the laser annealing process or initial surface condition, or both, rather than the cell processing.

3.2.2 n-Type Substrate With $11B^+$ Ion Implant Dopant

There was only one experiment with n-type substrates annealed with the large laser (Lucy). Material used was 0.9 ohm-cm phosphorus doped Cz wafers. The front junction side was $11B^+$ implanted at 10 keV with 1×10^{15} atoms/cm², and the back was $31P^+$ implanted at 50 keV with 1×10^{16} atoms/cm². (These wafers were from an unrelated project.) Laser energy density for the front and back was 1.2 J/cm² and 1.5 J/cm² respectively from the larger laser with 12% overlap. Average cell efficiency was 7% with poor V_{oc} due to insufficient emitter dosage that weakened the internal electric field (Table 3-8).

Two more experiments with n-type wafers were performed with the small (Exci-Lite) laser. Material used was 4" n-type Cz (1

Table 3-6. Small laser (Exci-Lite) annealing of Cz and FZ wafers. Ion implanted with $+P^{31}$ at 5 keV; 18-grid evaporated-type metallization; AR-coated. Cells measured at 25°C AM1.5 calibrated with JPL standard cell MT-472.

- a. Cz cell. Ion fluence = 1×10^{15} atom/cm²; laser energy density = 1.5 J/cm²; overlap = 50%; pulse duration = ~30 ns.

Cell ID	Sheet Rho (ohm/sq)	J _{sc} (mA/cm ²)		V _{oc} (V)		FF (%)		Eff (%)	
		Pre AR	Post AR	Pre AR	Post AR	Pre AR	Post AR	Pre AR	Post AR
B26-1E									
#1	80-90	21.24	31.74	0.584	0.598	78.76	78.26	9.76	14.85
#2	"	21.24	31.86	0.584	0.599	78.31	78.31	9.73	14.94
#3	"	21.37	---	0.585	---	76.57	---	9.57	---
#4	"	20.80	---	0.581	---	77.33	---	9.35	---

- b. Cz cell. Ion fluence = 2.5×10^{15} atom/cm²; laser energy density = 1.5 J/cm²; overlap = 50%; pulse duration = ~30 ns.

Cell ID	Sheet Rho (ohm/sq)	J _{sc} (mA/cm ²)		V _{oc} (V)		FF (%)		Eff (%)	
		Pre AR	Post AR	Pre AR	Post AR	Pre AR	Post AR	Pre AR	Post AR
B26-2.5E									
#1	44-48	21.44	31.79	0.596	0.610	79.44	79.50	10.15	15.4
#2	"	21.62	32.45	0.596	0.612	79.36	79.51	10.22	15.78
#3	"	21.32	32.06	0.594	0.610	79.74	79.63	10.10	15.57
#4	"	21.50	32.68	0.595	0.604	78.76	74.63	10.08	14.73

- c. FZ cell. Ion fluence = 5×10^{15} atom/cm²; laser energy density = 1.5 J/cm²; overlap = 50%; pulse duration = ~30 ns.

Cell ID	Sheet Rho (ohm/sq)	J _{sc} (mA/cm ²)		V _{oc} (V)		FF (%)		Eff (%)	
		Pre AR	Post AR	Pre AR	Post AR	Pre AR	Post AR	Pre AR	Post AR
B26-5E									
#1	66-75	19.94	---	0.579	---	75.65	---	8.71	---
#2	"	19.68	---	0.585	---	78.06	---	8.95	---
#3	"	20.22	---	0.588	---	79.01	---	9.15	---
#4	"	20.01	---	0.589	---	76.79	---	9.04	---
#5	"	20.08	---	0.587	---	77.32	---	9.11	---
#6	"	- - - Shunted - - -							

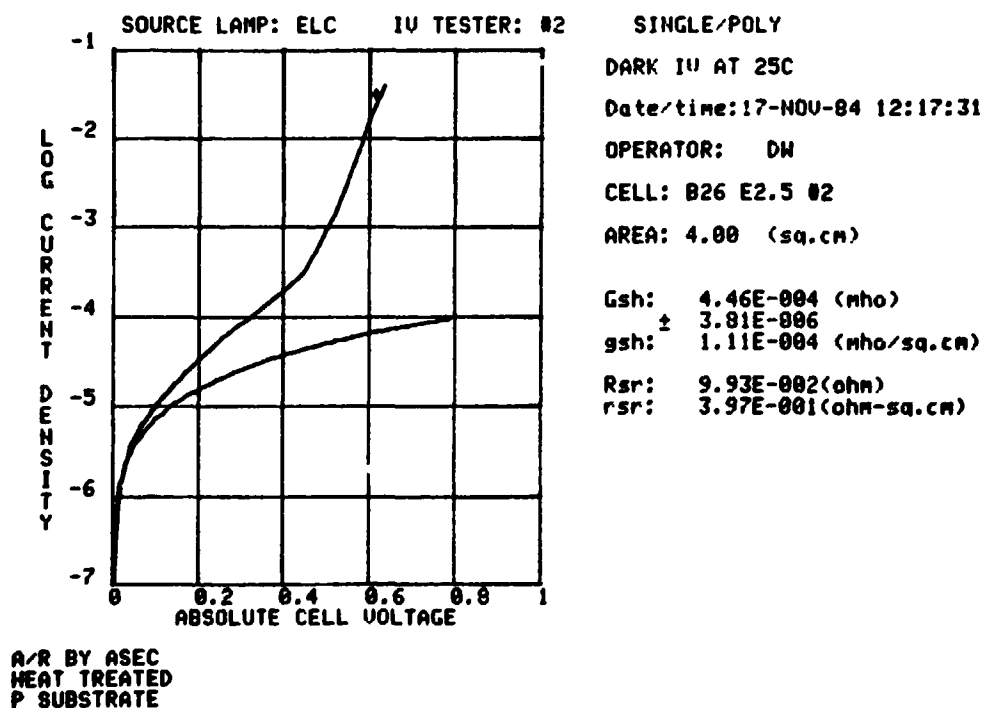
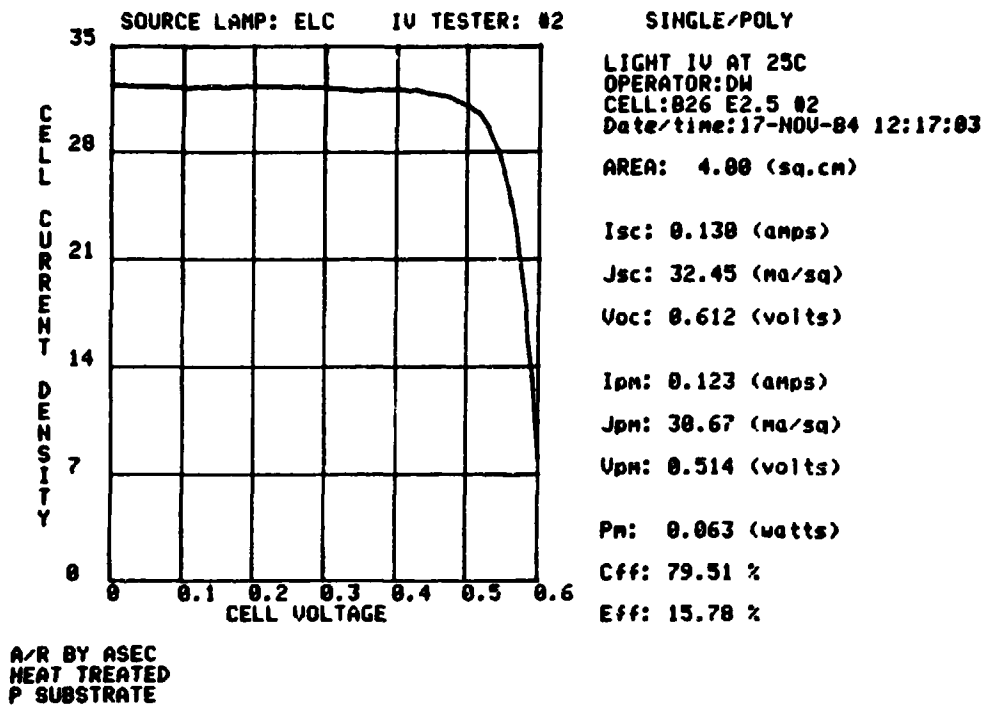


Fig. 3-4. I-V curves of best cell from B26-2.5E.

Sample: B26 2.5E15, A/R BY ASEC, HEAT TREATED #2.

Voltage: 0.000 Volts Light Bias: N

Date/time: 17-NOV-84 12:21:12 Operator: DM

System Calibrated 17-NOV-84 11:55:23 Standard Cell 0325

Data stored: CSR:QEJBT0/C2/B26_2E15_2_D0.DM

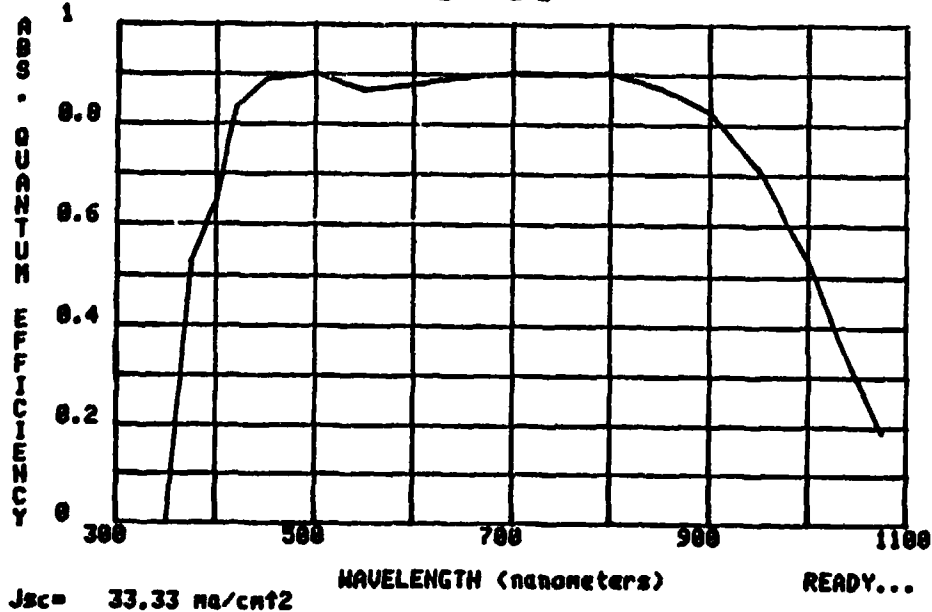


Fig. 3-5. Spectral response of best cell from B26-2.5E.

Table 3-7. ASEC-coated Cz cells; photolithographic gridlines. Implant energy = 5 keV; ion fluence = 2.5×10^{15} atom/cm²; laser energy density = 1.47 J/cm²; overlap = 50%; pulse duration = ~30 ns.

Cell ID	Sheet Rho (ohm/sq)	J _{sc} (mA/cm ²)	V _{oc} (V)	FF (%)	Eff (%)
B28 ASEC I					
#1	44-48	31.59	0.603	76.75	14.61
#2	"	31.42	0.605	79.09	15.04
#3	"	31.89	0.606	78.49	15.17
#4	"	31.22	0.606	80.46	15.23
B28 ASEC II					
#1	44-48	31.55	0.603	53.61	10.21
#2	"	31.98	0.605	75.71	14.66
#3	"	31.65	0.603	78.90	15.06
#4	"	31.13	0.597	74.89	13.93

Table 3-8. n-type substrates processed by large laser. $^{11}\text{B}^+$ ion implant on front at 10 keV, 1×10^{15} atom/cm²; $^{31}\text{P}^+$ ion implant on back at 50 keV, 1×10^{15} atom/cm².

Cell ID	Sheet Rho (ohm/sq)	J_{sc} (mA/cm ²)	V_{oc} (V)	FF (%)	Eff (%)
(N) B21					
#1	155 (front) 8 (back)	20.39	0.463	74.49	7.03
#2	"	19.51	0.460	73.65	6.61
#3	"	20.92	0.466	74.18	7.23

ohm-cm) 18 mils thick. The front side was $^{11}\text{B}^+$ ion implanted at 5 keV with a dosage of 2.5×10^{15} atoms/cm². After cleaning, the wafers were annealed at 1.52 J/cm² with 50% overlap for B27. The overall energy density was 1.43 J/cm² for B29. However, the beam for B29 was defocused in order to avoid the edge damage observed in B24 (Fig. 3-3). The backs were then coated with spin-on phosphorus dopant as the n^+ layer. Diffusion was done with a laser energy of 2.6-2.7 J/cm². Contacts were of the 18 gridline evaporated type. Some of the better cells were AR coated. Results are summarized in Table 3-9.

The highest efficiency obtained was 15% after AR (B27N #3). The current was higher than for a p-type substrate of 0.7 ohm-cm while the V_{oc} was lower. The poor result in B29, on the other hand, was a surprise. The only difference between B29N and B27N was the beam defocusing. The result was low J_{sc} , V_{oc} , and fill factor. Dopant depth profiling by spreading resistance technique on cells from these two experiments indicate that B27N had a junction of 0.28 micron and that B29N of almost 0.34 micron with a 0.15 micron thick "dead" layer (Fig. 3-6).

The difference in junction depth matched the lower J_{sc} obtained in the deeper junction (B29N) cells. However, it is not clear why B29N had a deeper junction than B27N since all parameters and materials are identical. It is possible that the defocused beam in B29N had much higher energy density at the center that drove the junction deeper. Also, nonuniform surface annealing that caused low V_{oc} and fill factor might have resulted from defocusing. The back surface sheet resistivity after annealing was about 8-9 ohms/square. Spreading resistance profiling indicated the presence of a sharp but deep n^+ junction.

Table 3-9. n-type substrates processed by small laser. Contacts were of the 18 gridline evaporated type. Ion implant energy = 5 keV; ion fluence = 2.5×10^{15} atom/cm²; overlap = 50%.

a. Laser energy density = 1.52 J/cm².

Cell ID	Sheet Rho (ohm/sq)	J _{sc} (mA/cm ²)		V _{oc} (V)		FF (%)		Eff (%)	
		Pre AR	Post AR	Pre AR	Post AR	Pre AR	Post AR	Pre AR	Post AR
B27N									
#1	53	22.03	31.73	0.583	0.595	77.68	77.84	9.98	14.70
#2	"	21.34	29.18	0.581	0.589	78.39	77.76	9.73	13.36
#3	"	22.02	32.68	0.582	0.597	77.21	76.93	9.89	15.00
#4	"	21.79	32.15	0.583	0.594	77.71	77.42	9.86	14.79

b. Laser energy density = 1.43 J/cm².

Cell ID	Sheet Rho (ohm/sq)	J _{sc} (mA/cm ²)		V _{oc} (V)		FF (%)		Eff (%)	
		Pre AR	Post AR	Pre AR	Post AR	Pre AR	Post AR	Pre AR	Post AR
B29N									
#1	50-53	19.54	---	0.570	---	76.25	---	8.49	---
#2	"	20.22	---	0.564	---	76.09	---	8.69	---
#3	"	20.38	---	0.569	---	75.13	---	8.71	---
#4	"	20.60	---	0.579	---	74.31	---	8.87	---

SPREADING RESISTANCE ANALYSIS

DATE 11/12/84 PROBE LOAD 5g ORIENTATION 11/12/84
 COUNTER 465631 SEIVEL ANGLE 0.0031
 SOURCE A F C O STEP INCR 2.5° SAMPLE = B29

SPREADING RESISTANCE ANALYSIS

DATE 11/12/84 PROBE LOAD 5g ORIENTATION 11/12/84
 COUNTER 465631 SEIVEL ANGLE 0.0031
 SOURCE A F C O STEP INCR 2.5° SAMPLE = B29

SPREADING RESISTANCE ANALYSIS

DATE 11/12/84 PROBE LOAD 5g ORIENTATION 11/12/84
 COUNTER 465631 SEIVEL ANGLE 0.0031
 SOURCE A F C O STEP INCR 2.5° SAMPLE = B29

Fig. 3-6. Depth profiles.

SECTION 4.0 DISCUSSION

4.1 LASER ANNEALING PROCESSING

In this quarter, it was found that when the beam of the smaller excimer laser was homogenized with a kaleidoscope, this laser was capable of processing cells not only to match those of the larger laser in cell efficiency, but also by an order of magnitude faster in process time; i.e., more economical and feasible for solar cell production implementation. However, because of being less uniform in beam quality, more overlap is required for complete surface annealing. The best Cz cell so far obtained was 15.8% without BSF and with standard 18 gridlines deposited through a shadow mask that caused 9% loss in active surface area. By incorporating an AR coating, an effective BSF and fine gridline structure, the maximum efficiency should exceed 16%. Limitations existing to higher efficiency are believed to be: (a) the detrimental effect of the overlap boundaries; (b) lattice damage by high keV ion implantation; and (c) surface cleanliness.

Overlap Boundaries. The overlap problems are related to laser beam quality, which is being continuously upgraded. The sequential slope of improvement to the beam quality and the corresponding cell efficiency in the last two quarters can be visualized from Fig. 4-1. It appeared that fewer demarcation lines would give higher cell efficiency. Figure 4-2 is a laser scan of a recent cell showing clearly the effect of edge damage by the laser beam. It was found that the edge damage could be eliminated by defocusing the beam to make it "fuzzy." However, this also resulted in nonuniform surface annealing as experienced in B29N.

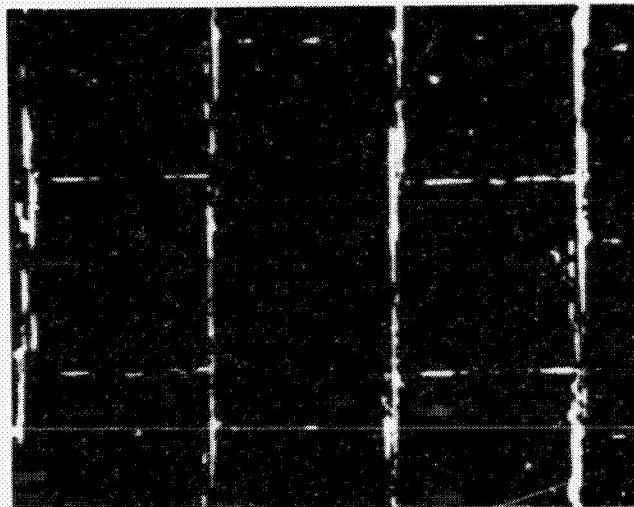
One of the other major factors that must be resolved is the beam output consistency. Although there has not been any misfires over several million shots, the beam intensity does not seem to be constant in processing from wafer to wafer. A second important factor was the pulse shape. The 30 nsec pulsation actually consisted of double peaks, one with higher intensity than the other. Although the exact cause of damage due to such dual-peak pulsation was not determined, preferentially etched surfaces revealed that more damage appeared on low/high pulse than on high/low pulse (Fig. 4-3). It is possible that the high intensity peak at the late pulse may produce vaporization.

Ion Implantation. After a series of experiments, it was found empirically that the best high efficiency cells were obtainable by 5 keV ion implant with fluence about 3×10^{15} atoms/cm². Decrease in lattice damage depth by implanted ions can be obtained by using non-mass analyzed glow discharge ion implantation at low keV (see Section 2.0). Lattice damage can be reduced further by implanting smaller atoms such as boron. Low

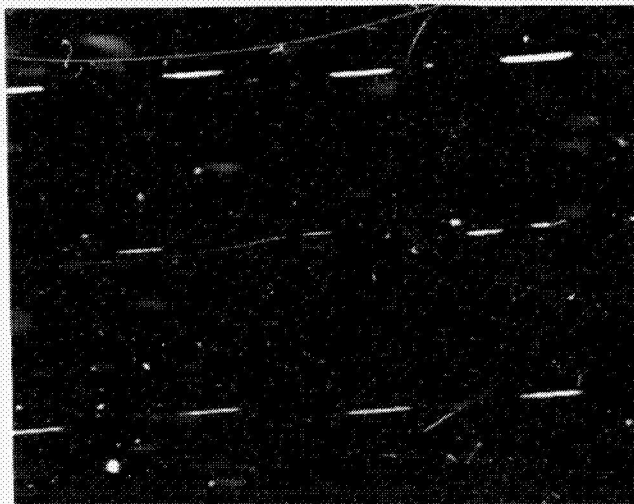
ORIGINAL PAGE IS
OF POOR QUALITY



July
6-7% (no AR)



September
9.8% (no AR)



October
15.8% (with AR)

Fig. 4-1. Decrease in beam demarcation lines during the past four months.

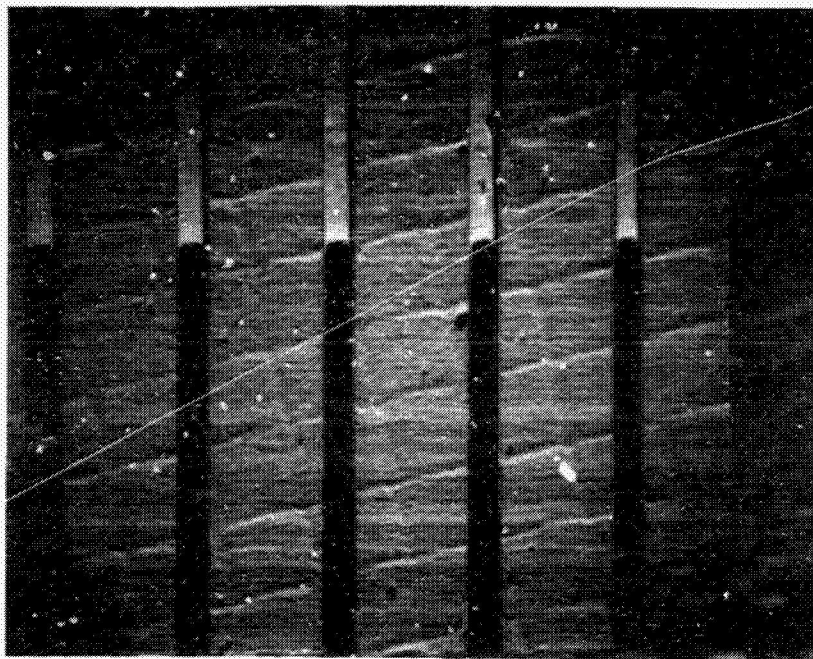


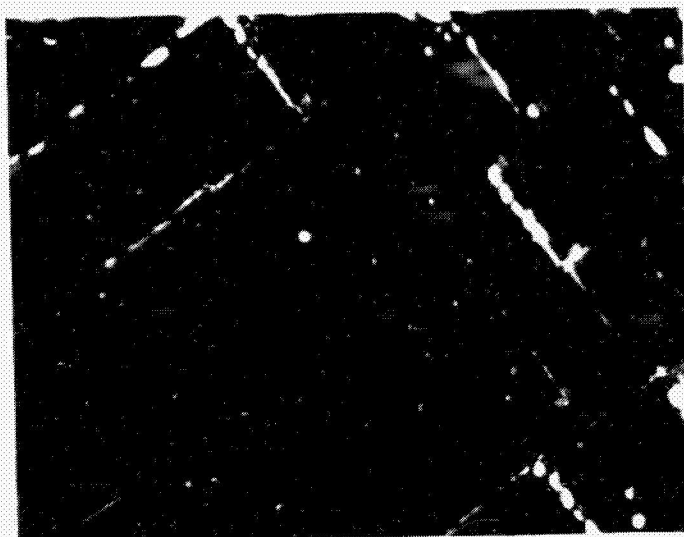
Fig. 4-2. Laser scan showing edge damage. Recent cell processed at 1.4 J/cm^2 , 50% overlap. Black dots are surface defects.

energy ion implant (1 keV) at high dosage fluence ($5 \times 10^{15} \text{ atoms/cm}^2$) should provide the maximum J_{sc} and V_{oc} .

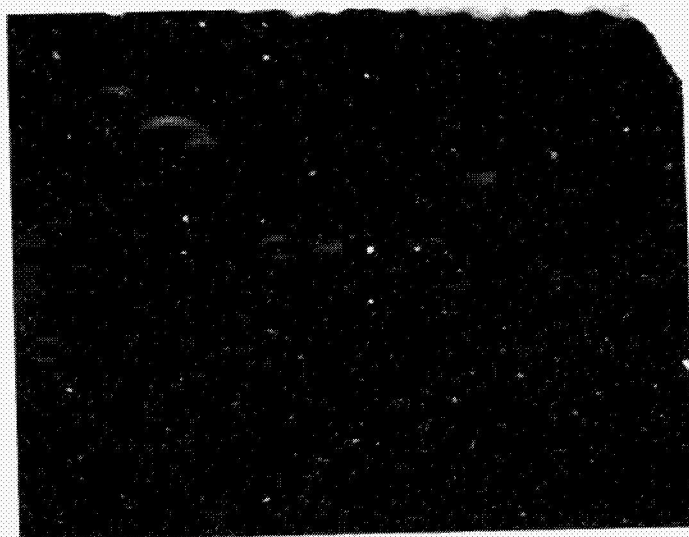
Surface Cleanliness. Lack of surface cleanliness has been observed to be one of the shunting sources that caused poor fill factor and low V_{oc} in laser annealed cells. The spots shown in Fig. 3-1 were Auger analyzed. Contaminants found included oxygen, carbon, and calcium. This is a representative dust or water particulate, which may not be harmful for conventional furnace diffusion because of the low temperature (850°C) solid state diffusion process. For laser annealing, however, the diffusion is a liquid-solid phase type. The surface is at melting temperature (in nano seconds). Any carbonaceous or calcium deposit would become a nucleus for recrystallization. Such particulates are not always removable by traditional cleaning solutions. Wafer scrubbing by acid etching followed by 16 meg-ohm filtered (0.2 micron) deionized water rinsing has been found to provide a much cleaner surface condition. Both V_{oc} and fill factor have been improved by following this procedure.

To achieve cell efficiencies over 16%, an effort to include surface passivation, fine gridline metal deposition, and an effective BSF will be made. Before the gas cell is completed, surface passivation will be performed by thermal oxidation and fine gridlines will be formed by photolithography. BSF experiments will be performed with an ion-implanted back surface

ORIGINAL PAGE IS
OF POOR QUALITY



a. Low-high pulse.



b. High-low pulse.

Fig. 4-3. Damage caused by various pulse shapes.

and with a spin-on source which is economical and fast.

4.2 SUBSTRATES: p OR n TYPE

So far in the program, p-type low resistivity (0.7 ohm-cm) material has been used extensively in order to avoid the additional BSF process. The trade-off was the decrease in J_{sc} . Achievement of 35 mA/cm² in J_{sc} is facilitated by use of high resistivity material. An effective BSF can compensate for the V_{oc} . One of the conventional methods is to sinter aluminum paste at 850°C. However, the sintering could degrade the bulk minority lifetime, electrically deactivate the emitter dopant concentration (S. R. Wilson et al., 1983) and induce thermal/mechanical stress. To avoid the problems, n^+ could easily be diffused by using phosphorus liquid dopant driven in with a high energy density excimer laser. This experiment was conducted with B29N. The sheet rho at the back before and after n^+ diffusion was 30 ohms/square and 8 ohms/square respectively. Spreading resistance dopant profiling suggested the n^+ layer was more than 0.5 microns deep (Fig. 3-6). The BSF effect was not observed in the cell due to the cell thickness (over 18 mils). To drive boron or aluminum into silicon from a liquid dopant source is much more difficult. This was first observed early in this program and later reported by Westinghouse (R. Campbell, 1984). Therefore, n-type base material is preferable due to the easy n^+ implementation at the back. Ion implantation followed by laser annealing is an alternate method for n^+ formation except the cost is higher and vendor-dependent.

In the next quarter, both p and n substrates of high resistivity will be tested with aluminum paste, phosphorus liquid dopant, and ion implant for BSF implementation.

SECTION 5.0

PROCESS SELECTION REVISION AND SENSITIVITY ANALYSIS

Based on the work conducted so far, it is possible to re-examine and revise the proposed process sequence for fabricating cells in production. The revision of the process reflects the dependence on cell performance found by varying different process variables. In the next two sections, the revised process is outlined and a sensitivity assessment is made.

5.1 REVISED PROCESS

The most important change in the process sequence is the use of a smooth silicon surface rather than a textured surface for the wafers. The use of a textured surface was proposed in order to avoid a final anti-reflection coating to reduce reflection losses after encapsulation. However, excimer laser junction formation on these two types of surfaces showed that greater uniformity and performance could be obtained on smooth surfaces. The reasons for this will be discussed in the next section. As a result, the process proposed in Fig. 25 in the first Quarterly Report is modified as reflected in Fig. 5-1 in order to use smooth-surfaced Cz wafers.

In the revised process, as-sawn wafers are etched in 30% NaOH to remove surface damage from sawing and to produce a sufficiently smooth surface to allow uniform laser processing. Following the damage etch, the surface is cleaned in dilute sulfuric acid, rinsed, and dried. The ion implanting is carried out at a fluence of 2.5×10^{15} atoms/cm² of $11B^+$ at an energy of 5 keV. The surface requires careful preparation before laser junction formation. The reasons for the preparation are described in the next section. This process includes an HF etch followed by a spin/scrubbing rinse followed by spin dry. This treatment is necessary in order to remove so-called "water spots." Following the surface cleaning, the dopant is activated and the junction formed by XeCl excimer laser processing at 1.5 J/cm² at 50% overlap. The pulse length is 20-30 nsec. The processing steps until contact buildup remain the same as described previously. After the contacts are completed, a belt furnace AR coating step is performed. From this point, the cells are tested, sorted, and sent to module assembly.

5.2 PROCESS SENSITIVITY ASSESSMENT

The key parameters that control the quality of the solar cells made using an excimer laser junction formation process step are: type and resistivity of incoming wafer; wafer surface condition; ion implant energy, fluence, and uniformity; surface cleanliness before laser "annealing"; laser processing uniformity, overlap, energy density, pulse length, and pulse shape; metallization process, and AR coating. In the following paragraphs, the

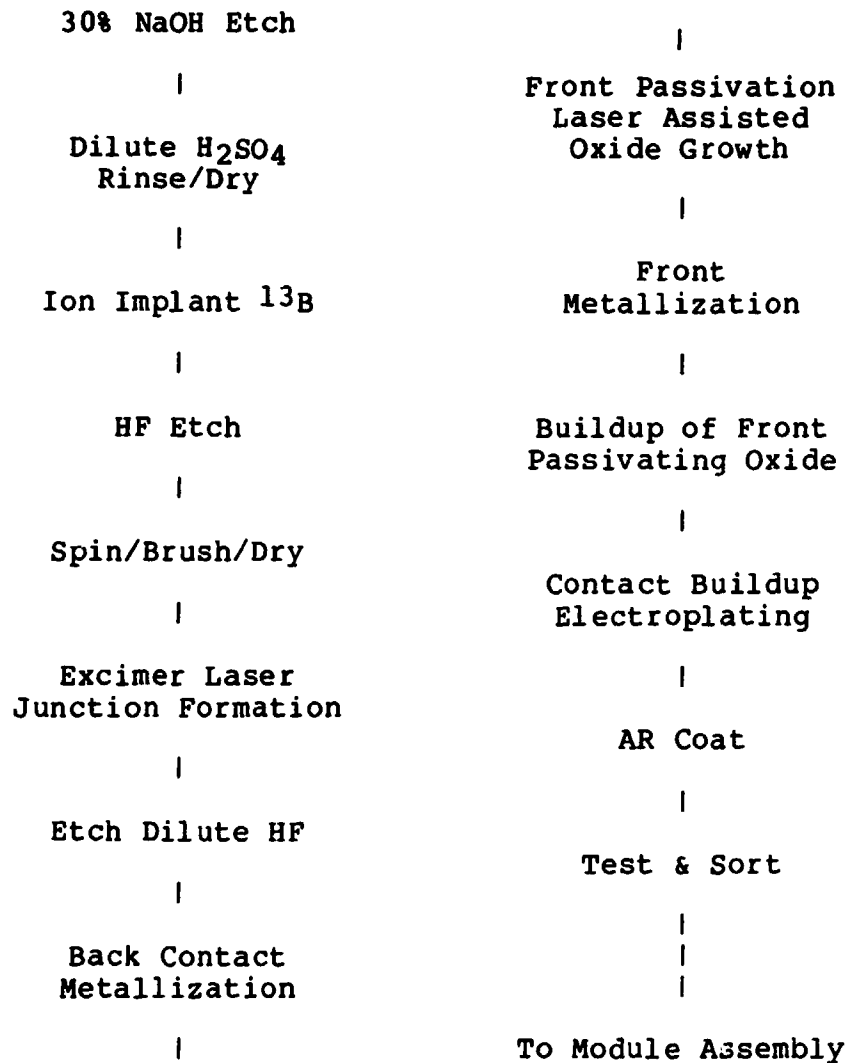


Fig. 5-1. Revised excimer laser process.. 5.2" diameter p-type (boron-doped) 0.7 ohm-cm Cz silicon.

sensitivity found in cell performance and yield will be discussed as a function of these variables.

Wafer Type and Resistivity. Most of the work carried out in this project has been on p-type Cz material in the range of 0.3 to 0.8 ohm-cm. P-type material has been used because the resistivity variation in 36" ingots normally grown is much smaller than that found in n-type Cz growth, a factor of approximately 2:1 compared with 4:1 due to the differences in segregation efficiency of boron and phosphorus dopants. This allows good control on the wafer diffusion lifetime over large volume production. No BSF process is necessary for such low resistivity material, 0.3-0.7 ohm-cm.

Surface Morphology. Early in the project, experiments were carried out to assess the potential of using textured surfaces for laser junction formation processing. It was found that significantly lower energy densities were required to obtain junctions than for chem-mech polished (CMP) surfaces. Energy densities on the order of 0.3-0.5 J/cm² were found to be sufficient. These values are 20-25% of those required for CMP surfaces. The effective energy densities were greater because of multiple reflections at the pyramidal surfaces. However, these surfaces were much more susceptible to laser-induced damage because energy density nonuniformities are multiplied by the multiple reflections. Overlap effects were much more pronounced also for the same reasons. Based on these considerations, the proposed process has been modified to use chemically smoothed surfaces such as those produced by concentrated sodium hydroxide etches. All of the work done so far has been on CMP surfaces in order to provide a well controlled substrate condition. Chemically polished (CP) surfaces will be evaluated during the next quarter.

Ion Implantation. Along the lines of the work of Young, Wood, and colleagues, it has been found in this study that the implant energy and fluence are key variables for the production of the highest efficiency cells. Cells made from 10 keV implant energy were found to be lower in efficiency than those fabricated at 1 or 5 keV. The results of this project show so far that there is little difference in the performance of cells made with implants of 1 or 5 keV. Young et al. found that junction depths of 0.15 micron could be obtained with glow discharge implants at 1 keV. The short circuit current densities for these cells were 35.7 mA/cm² after AR coating, as expected for such shallow junctions. The best cells made in the present study with 5 keV implant energy have yielded current densities of 32.7 mA/cm², which is attributed to the lower current density expected with junctions on the order of 0.25-0.30 micron. The performance of cells made with 1 keV implant energy on a modified ion milling machine has been poor because of nonuniformity problems in the dopant distribution. A key problem in obtaining the highest efficiencies on a production basis is the lack of a commercially available implanter in the energy range of 0.8-2 keV with

sufficient ion current density, deposition area, and uniformity.

The dose level or fluence is another important parameter since it determines the resistivity of the surface and junction field after laser processing. The best cells are made with a sheet rho of 60-70 ohms/sq and a surface concentration of $2.5-3.0 \times 10^{15}$ atoms/cm². Lower concentrations yield high sheet rhos (>100 ohms/sq) which cause degradation of performance due to series resistance and weak built-in junction voltage (V_{bi}), while higher concentrations produce profiles with a maximum 0.03-0.05 micron deep in the dopant distribution. This appears to lower the collection efficiency as shown by lower currents.

Laser Processing Overlap. Two processing regimes appear to be possible, depending on the type of beam spot overlap scheme used. The two regimes are characterized as the minimum overlap and maximum overlap. In the minimum overlap regime, the best results are obtained when overlap in both scan directions is made as small as possible, preferably less than 2-5%. The work by the Oak Ridge National Lab group has been primarily in this regime. A key requirement for good results in the minimum overlap regime is excellent beam uniformity and sharp beam edge shape. On an area basis, these requirements are optimized by the use of a large area beam laser in order to minimize the beam-perimeter-to-cell-area ratio. In the maximum overlap regime, the best results are obtained when the laser beam overlaps 50% in both scan directions, resulting in each unit area being hit by four laser pulses. This regime minimizes the importance of beam non-uniformities over both the beam area and at the edges. In addition, the requirement for large beam area lasers is lessened so that high pulse rate, lower energy lasers can be used. In a later part of this project, the economic consequences of the utility of these two regimes will be carefully examined.

So far in this project, little difference in the performance of cells fabricated using these two regimes has been found. After optimization of the fabrication parameters, cells of equivalent performance have been made, although the best cells have been made in the maximum overlap regime since, until this time, the best cells have been made with 5 keV implant energies. These energies drive the ions in to 0.25 micron or so. Thus the overlap experiments so far have not unraveled the dependence of junction depth and J_{sc} on overlap.

Energy Density and Pulse Duration. For the annealing of p type material with ³¹P ion implant the range of 1.3-1.6 J/cm² has been found to be a broad range of energy densities for which proper junction formation can take place. The best results in this study center in the range of 1.45-1.55 J/cm². This range assumes an implant energy of 5 keV. The pulse duration can be in the range of 25-30 nsec. Higher energy densities create defects as shown by etch experiments. Lower energy densities inadequately distribute and activate the implanted dopant. These results

compare well with those found in previous studies. Lower implant energies may require laser beam energy densities of 1.4 J/cm^2 . Pulse shape is an important variable. If the pulse has several maxima, better results are obtained if the maxima come in a high-low sequence. This order minimizes defects induced on the surface. Ideally the pulse shape should be "flat-top" in respect to the switch on time.

Uniformity. The two important type of uniformity are the area uniformity and the edge region uniformity. Laser beam intensity uniformity distribution on the order of 5-10% appears to be adequate for the production of cells when the pulse length and shape have been optimized as mentioned above. The required uniformity can be obtained using optical transformations on relatively non-uniform beams. The more critical uniformity issue is related to the type and extent of damage left at the edges of the beam where overlap occurs. In the minimum overlap regime, beam alignment and sharp beam edge roll-off are important. The alignment obtained by standard X-Y translation stages is adequate and allows registration of the edges to within 0.001 inches (0.0254 mm). The dependence of cell performance on beam edge sharpness has been more difficult to assess. A roll-off of 45%/10 micron gives approximately 90% roll-off in 30 microns which gives the best cells obtained in the minimum overlap region. For small beam size, (0.6x0.8 mm), this corresponds to 7% overlap. In the maximum overlap region beam roll-off is relatively unimportant and beam area uniformities of 7-10% give optimal performance in cell yield. The obvious trade-off for 50% overlap is the four fold reduction in processing rate. In the economic evaluation phase of the project the economic consequences of these considerations will be made.

Metallization and AR Coating Processes. The high sheet rho obtained with the shallow junctions employed in laser processed cells, in the range 60-80 ohms/square, require an effective fine line metallization pattern to minimize the distance of current flow to the collector and to minimize area coverage. The use of 25 line/cm patterns with 3-4% area coverage will be required to optimize current collection. Because the surfaces processed are smooth an AR coating will be required to minimize reflection losses. Encapsulated cells should be optimized with a single layer AR coating.

SECTION 6.0

CONCLUSION

It has been demonstrated in the last quarter that a high efficiency Cz cell can be processed without using a large spot size, high power excimer laser. The important factors that contributed to the result included beam homogenization, surface condition, and appropriate, though not yet optimized, ion implant parameters.

To achieve cell efficiencies over 16%, an effort to include surface passivation, fine gridline metal deposition, and an effective back surface field will be made. Before the gas cell is completed, surface passivation will be performed by thermal oxidation and fine gridlines will be formed by photolithographic metal deposition. BSF experiments will be performed with ion implantation and with spin-on sources.

SECTION 7.0 PROBLEMS AND PLANS

7.1 PROBLEMS

1. Damage at beam edge is believed to cause reduction in V_{oc} . There is no immediate method to eliminate such line defects.
2. Low keV ion implantation by glow discharge will input a new parameter that requires time for its optimization.
3. Laser-assisted fine gridline deposition is anticipated with problems of slow deposition rate, surface adhesion, and plate-up process development.

7.2 PLANS

1. Produce 16.5% Cz cells.
2. Test and implement glow discharge implantation and laser-assisted CVD gridline deposition.

Program Tasks

I. Program Management

- a. Subcontract Approval
- b. Management

II. Process Selection

- a. Target Process
- b. Revision
- c. Final Process Specification

III. Process Development

- a. Annealing Study
- b. Equipment Fabrication
- c. Experimental Matrix
- d. Deliver 25 2x2 cm cells

IV. Process Sensitivity Assessment

V. Process Verification

- a. Cell Processing
- b. Cell Characterization
- c. Deliver 25 5.2" cells

VI. Laser Reliability and Appropriateness

VII. Cost Evaluation

VIII. Documentation

- a. Program Plan
- b. Laser Process Selection Report
- c. Economic Analysis Report
 - Preliminary
 - Final
- d. Monthly Progress Reports
- e. Quarterly Progress Reports
- f. Final Report
 - Draft
 - Final (one month after JPL comments)
- g. Program Reviews as Required
- h. PIM

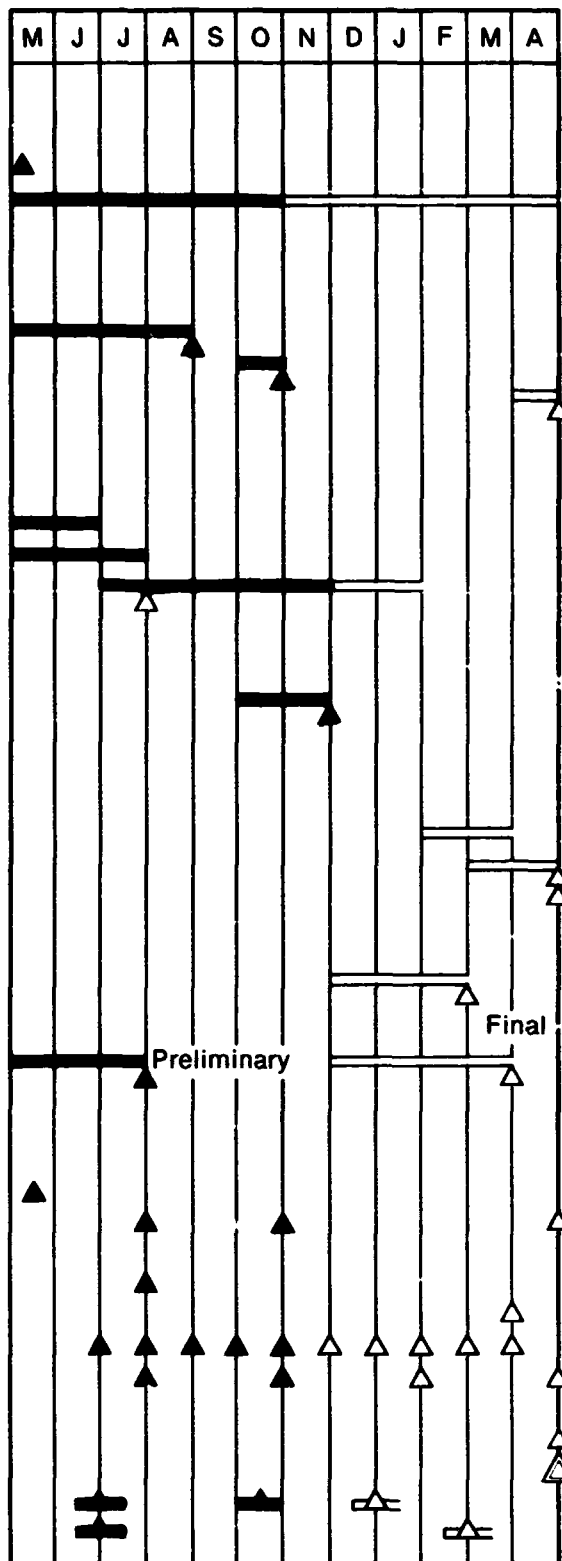


Fig. 7-1. Program schedule.

REFERENCES

1. Robert Campbell. Westinghouse report presented at JPL Project Integration Meeting, 1984.
2. S. R. Wilson, W. M. Paulson, R. B. Gregory, G. Tam, C. W. White, B. R. Appleton, A. K. Rai, and P. P. Pronko. "Thermal Stability of Electrically Active Dopants in Laser Annealed Silicon Films." J. Applied Physics, 54 (9), 5004-13, Sept. 1983.
3. R. T. Young, J. Narayan, W. H. Christie, G. A. van der Leeden, J. I. Levatter, and L. J. Cheng. "Semiconductor Processing with Excimer Lasers." Solid State Technology, 26 (11), 183-9, Nov. 1983.
4. R. T. Young, G. A. van der Leeder, R. L. Sandstrom, F. F. Wood, and R. D. Westbrook. Appl. Phys. Lett. 43 (7), 666, 1983.

ACKNOWLEDGMENTS

Assistance and continuous encouragement from Paul Alexander is highly appreciated. Technical assistance from Bruce Love, Frank Uno, and Joe Russo has been most helpful. The authors would also like to thank Dorothy Houk, Jim Wilson, Mari Kristiansen, and Mary McLaughlin for assistance in completing this report.